Part II
Geological Hazards

Peter Webley

Editor-in-Chief

6

Building an Uncertainty Modeling Framework for Real-Time VATD

Peter Webley,[1] Abani Patra,[2] Marcus Bursik,[3] E. Bruce Pitman,[4] Jonathan Dehn,[1] Tarung Singh,[2] Puneet Singla,[2] Matthew D. Jones,[5] Reza Madankan,[2] E. Ramona Stefanescu,[2] and Solene Pouget[3]

ABSTRACT

When forecasting the future location of volcanic-ash clouds, uncertainties exist in the input parameters used in dispersion modeling and in the weather prediction data used for modeling the advection terms. Recent developments have shown that probabilistic modeling provides the tools to assess the variability in downwind ash concentrations. We show a probabilistic modeling approach where ensembles of forecasts are generated from a suite of simulations using a coupled one-dimensional plume model and a Lagrangian dispersion model. This approach produces charts of the probability of ash-cloud concentrations and mass loadings exceeding user-defined thresholds. We focus on the initial plume uncertainties and discuss how uncertainties in numerical weather prediction data could also be applied within our approach. Our results show how, by assigning the initial likelihoods of input parameters, the probabilistic approach can produce mean ash concentrations and mass loadings as well as probabilities of breaching a defined threshold. We show how, given the variability in the inputs, the probabilistic modeling can be used to assess the confidence in the ash-mass loadings. This is critical for real-time volcanic-hazard assessment and our approach illustrates how a new tool could be developed for those in decision support.

6.1. INTRODUCTION AND BACKGROUND

Volcanic-ash plumes and dispersing clouds can be a hazard to both the aviation community and population centers downwind of the volcano [*Horwell and Baxter*, 2006; *Prata and Tupper*, 2009]. Operational organizations, such as Volcanic Ash Advisory Centers (VAACs), simulate the clouds' future location for use in their decision-support systems. Then volcanic ash advisories [VAA; see within *ICAO*, 2012] can be generated for the aviation industry. Also, fallout advisories often provided by local volcano observatories can provide advice on the potential impact to human health (see *Horwell and Baxter* [2006] for more on impact of volcanic ash on human health). To forecast the ash plumes' and clouds' future position and concentration levels, volcanic-ash transport and dispersion (VATD) models have been used. These VATD models are being used in either an operational setting to produce the cloud forecasts required for the VAACs' VAA [*Met Office*, 2012; *JMA*, 2014] (Fig. 6.1a), or in a research mode [see *Witham et al.*, 2007; *Webley et al.*, 2009a,b, 2010; *Folch et al.*, 2012] to

[1] Geophysical Institute, University of Alaska Fairbanks, Fairbanks, Alaska, and Volcanic Ash Detection, Avoidance and Preparedness for Transportation (V-ADAPT), Inc., Fairbanks, Alaska, USA
[2] Department of Mechanical and Aerospace Engineering, University at Buffalo, SUNY, Buffalo, New York, USA
[3] Department of Geology, University at Buffalo, SUNY, Buffalo, New York, USA
[4] Department of Mathematics, University at Buffalo, SUNY, Buffalo, New York, USA
[5] Center for Computational Research, University at Buffalo, SUNY, Buffalo, New York, USA

Natural Hazard Uncertainty Assessment: Modeling and Decision Support, Geophysical Monograph 223, First Edition.
Edited by Karin Riley, Peter Webley, and Matthew Thompson.

(a)

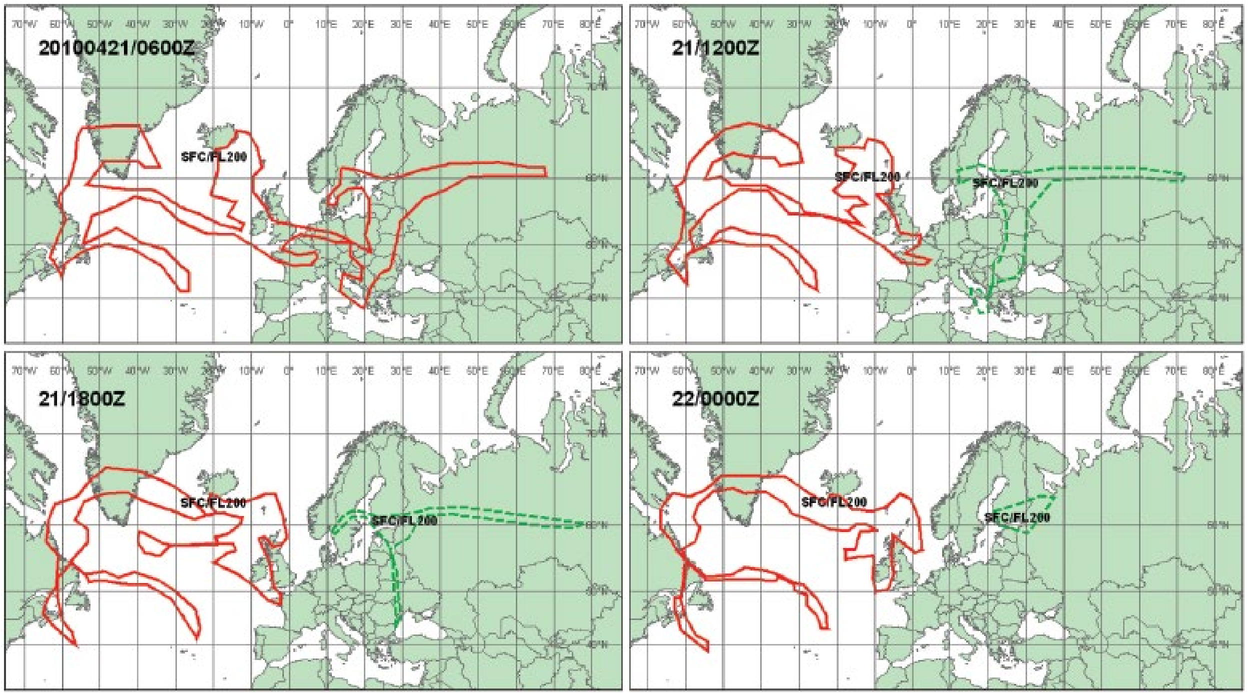

VA ADVISORY
DTG: 20100421/0600Z
VAAC: LONDON
VOLCANO:
EYJAFJALLAJOKUL 1702-02
PSN: N6338 W01937
AREA: ICELAND

SUMMIT ELEV: 1666M
ADVISORY NR: 2010/029
INFO SOURCE: ICELAND MET OFFICE
AVIATION COLOUR CODE: RED
ERUPTION DETAILS: ERUPTION CONTINUING
TO AROUND FL120 TO FL160.

RMK: NO SIG ASH ABOVE FL200. ASH CONCENTRATIONS UNKNOWN
THE TWO PLUMES ON 21/1200Z, 21/1800Z AND 22/0000Z CHARTS ARE
BOTH AT SFC/FL200.
NXT ADVISORY: 20100421/1200Z

(b)

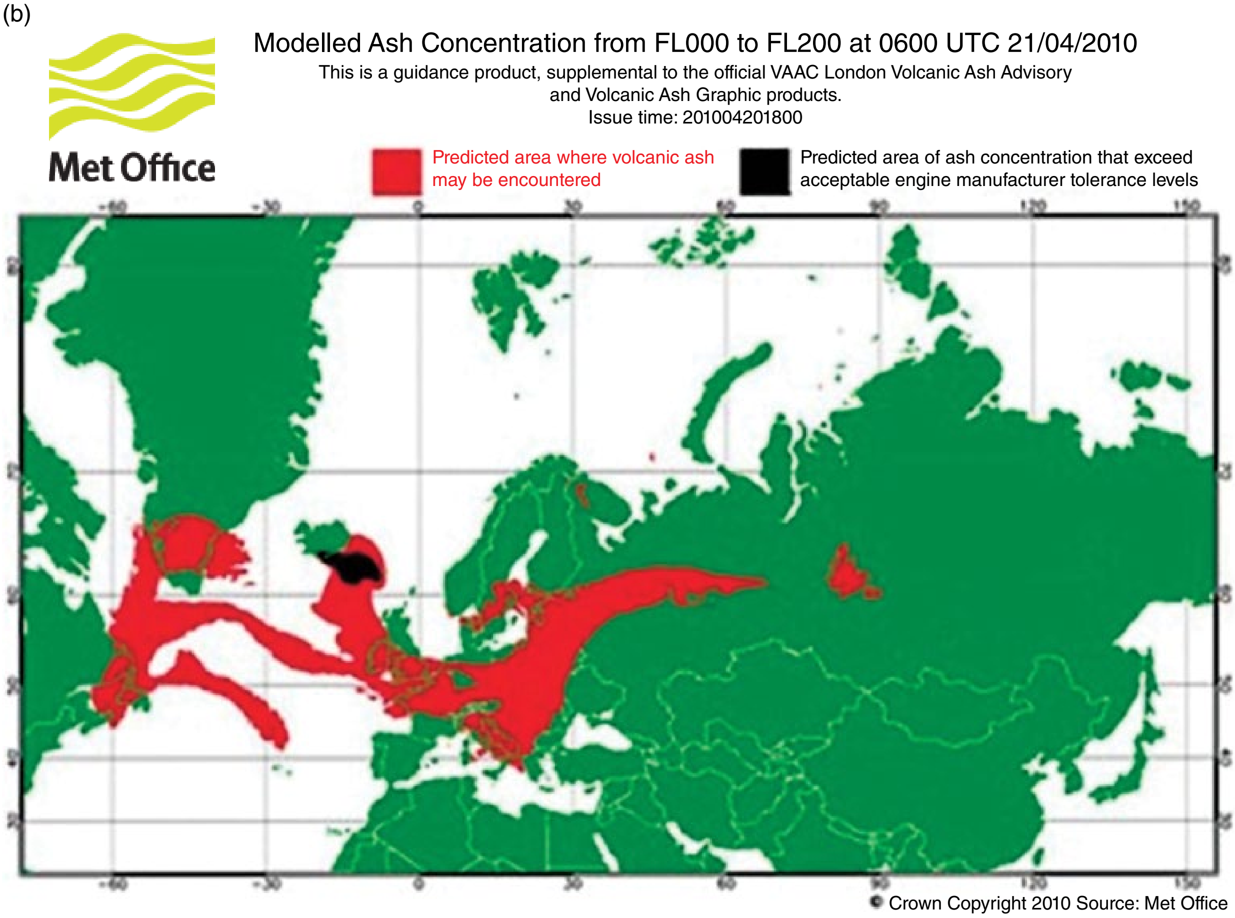

Figure 6.1 (a) London VAAC's VAA produced during Eyjafjallajökull eruption on 14 April 2010; (b) additional concentration product from the same date at 06:00 UTC; and (c) the progression to concentration thresholds during the Grimsvotn eruption on 25 May 2011.

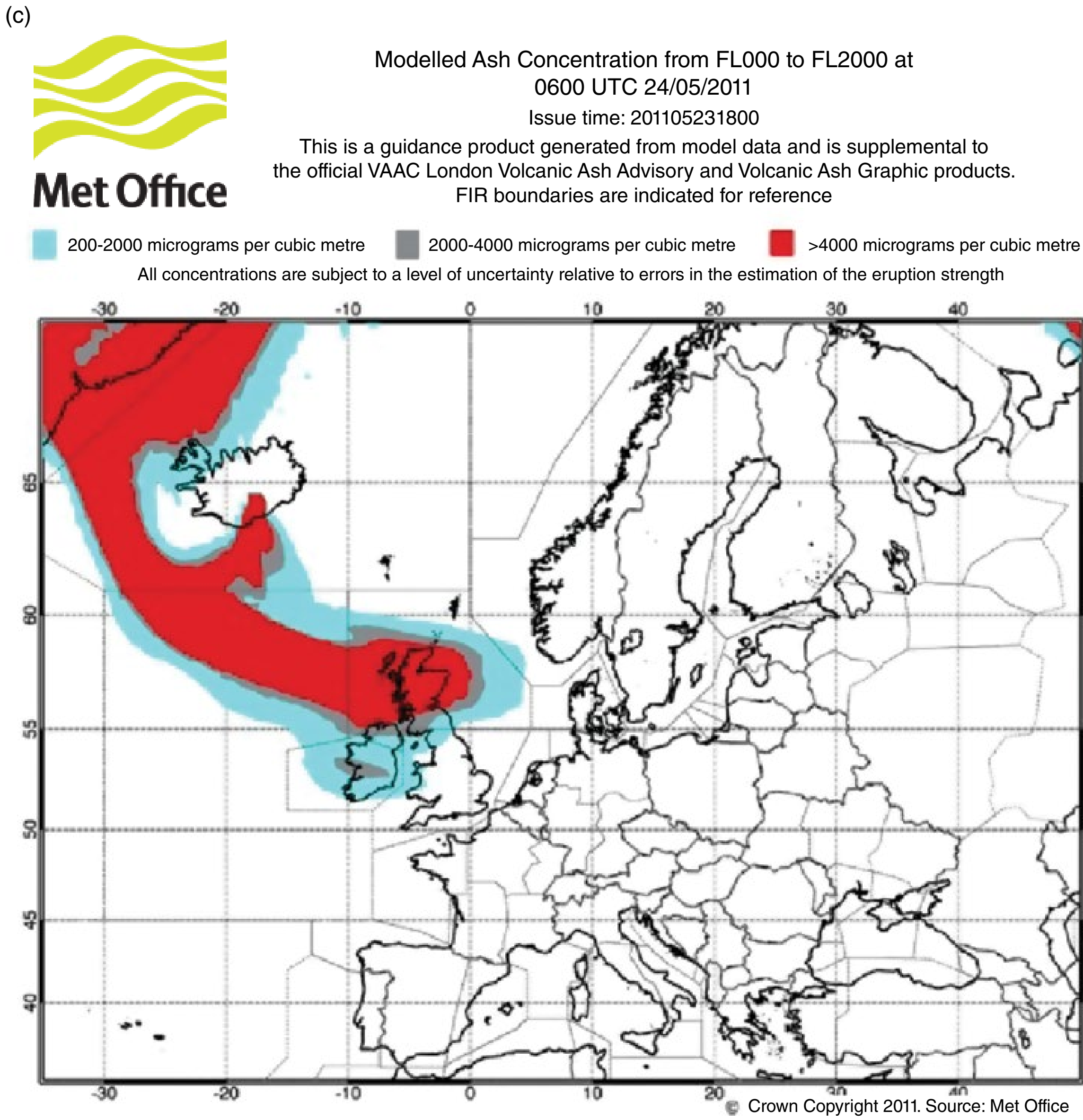

Figure 6.1 (Continued)

better understand the volcanic event and develop new processing algorithms and analysis tools for future volcanic-hazard assessment.

The eruption of Eyjafjallajökull volcano in 2010 [*Gudmundsson et al.*, 2010, 2012] illustrated the uncertainties that exist in performing volcanic-ash plume and cloud modeling in a real-time environment. The operational VAAC for the region produced, in addition to its standard VAA (Fig. 6.1a), a nonoperational product (Fig. 6.1b) that displayed the ash-cloud concentrations that exceeded aviation engine tolerance levels. These products were the result of a deterministic model simulation from one set of input parameters and used one deterministic numerical weather prediction (NWP) model. During the eruption of Grimsvotn in 2011 [*Tesche et al.*, 2012], the concentration forecast changed to display thresholds of 0–2 mg/m^3, 2–4 mg/m^3, and > 4 mg/m^3 (Fig. 6.1c). These were at the time deemed as acceptable by aircraft-engine manufacturers so there would be no or minimal risk of immediate damage to any aircraft [*Guffanti and Tupper*, 2014]. Uncertainties in plume-height estimation, vertical plume shape, initial particle- or grain-size distribution (PSD or GSD), event length, and mass eruption rate indicate that the potential range of the input parameters can vary on scales greater than the sensitivity of the concentration thresholds. Thus, the research and operational communities [*WMO*, 2010a, 2010b] held discussions on the need to progress toward adding probabilistic ash-cloud modeling to the deterministic forecasting that would place exceedance threshold estimates in proper context and allow better decision making.

Since the end of the International Civil Aviation Organization (ICAO) lead international volcanic-ash task force (IVATF) in 2012 [*ICAO,* 2012], there has been a progression toward probabilistic VATD modeling environments. These incorporate both the uncertainties in the model inputs [e.g., *Bursik et al.*, 2012] and the potential variability in the NWP [e.g., *Stefanescu et al.*, 2014; *Vogel et al.*, 2014]. Observational data from ground measurements [*Schneider and Hoblitt,* 2013], airborne campaigns [*Weber et al.*, 2012], and satellite remote sensing data [*Ellrod et al.*, 2003; *Pavolonis et al.*, 2013] can then be used to constrain these approaches through inverse modeling [e.g., *Madankan et al.*, 2014].

In this chapter, we present a new modeling approach that incorporates the uncertainties in the volcanic eruption initial conditions and the stochastic nature of the NWP data to generate a volcanic-ash-cloud forecast with associated probabilistic estimates in the location and four-dimesional concentrations (x, y, z, and t). We focus only on the input variability in this paper. We couple the Puff VATD model [*Searcy et al.*, 1998], to a one-dimensional model for plume rise called BENT [*Bursik*, 2001], which we refer to as Puffin. This approach provides the uncertainty estimates in the initial conditions of the eruption volcano. We have developed a sophisticated workflow that builds probabilistic Puff model simulations for a range of inputs from the Puffin tool. We will provide, in this chapter, an overview of the developed workflow focusing on one NWP dataset and illustrate some of the output products available that can then be used to compare to any available observational data.

6.2. METHODOLOGY

6.2.1. Probabilistic Modeling Workflow

Our approach incorporates eruption and NWP variability and uncertainty together to provide a probabilistic estimate of the ash-cloud location and concentration downwind of the volcano. Just as the Puff VATD model is able to analyze past volcanic eruptions using reanalysis [*Webley et al.*, 2012] and hindcast [*Steensen et al.*, 2013] data, our tool is applicable for past eruptive event analysis as well as for real-time model simulations for use in operational decision making. The workflow (Fig. 6.2) demonstrates how the source parameter uncertainty is applied to the BENT-Puff (Puffin) tool to build a set of dispersion model simulations/ensemble members. The mean and covariance of this set of simulations are updated by assimilating any available observational data (i.e., a satellite data) to then produce a posterior mean and covariance of the uncertain parameters (see *Madankan et al.* [2014] for more details).With each available satellite dataset, a new source parameter input distribution would be generated. With subsequent iterations, the workflow reduces the uncertainties in the inputs and hence produces a simulated ash-cloud product with higher confidence levels for the location and downwind concentrations. If no satellite data are available, then simulations with the prior input parameters are used for the full model simulation.

In the initial phase of the workflow, any input parameter for the BENT model can be defined with its associated variability. If observational data are available, such as eruption height from ground or space-borne observations, then the initial weightings can be edited to reflect the recorded plume height. We currently chose four parameters: vent diameter, vent velocity, mean particle size (log scale), and standard deviation of the size distribution (using a Gaussian shape centered on the mean particle size). For these four parameters, a set number of simulations are defined that target the potential range of each parameter with each simulation given an associated weight based on a minimization of the moments in the probabilistic analysis. More details on the definition of the methodology can be found in *Patra et al.* [2013], *Madankan et al.* [2014], and *Stefanescu et al.* [2014].

6.2.2. Near-Real-Time Processing Routines

In addition to the overall workflow design, we have built a set of processing routines to complete the probabilistic modeling in near real-time (NRT; Fig. 6.3). Given the start time and date, the routines download data from the closest radiosonde to the volcano's location extracting vertical profiles of temperature, wind speed, and relative humidity, at either 00 or 12 UTC depending on the start time for the simulations. These will be updated to use NWP to determine the atmospheric conditions at the volcano. Next, the routine builds the template for the Puffin tool. For our current setup in Fig. 6.3, we use four parameters to represent the

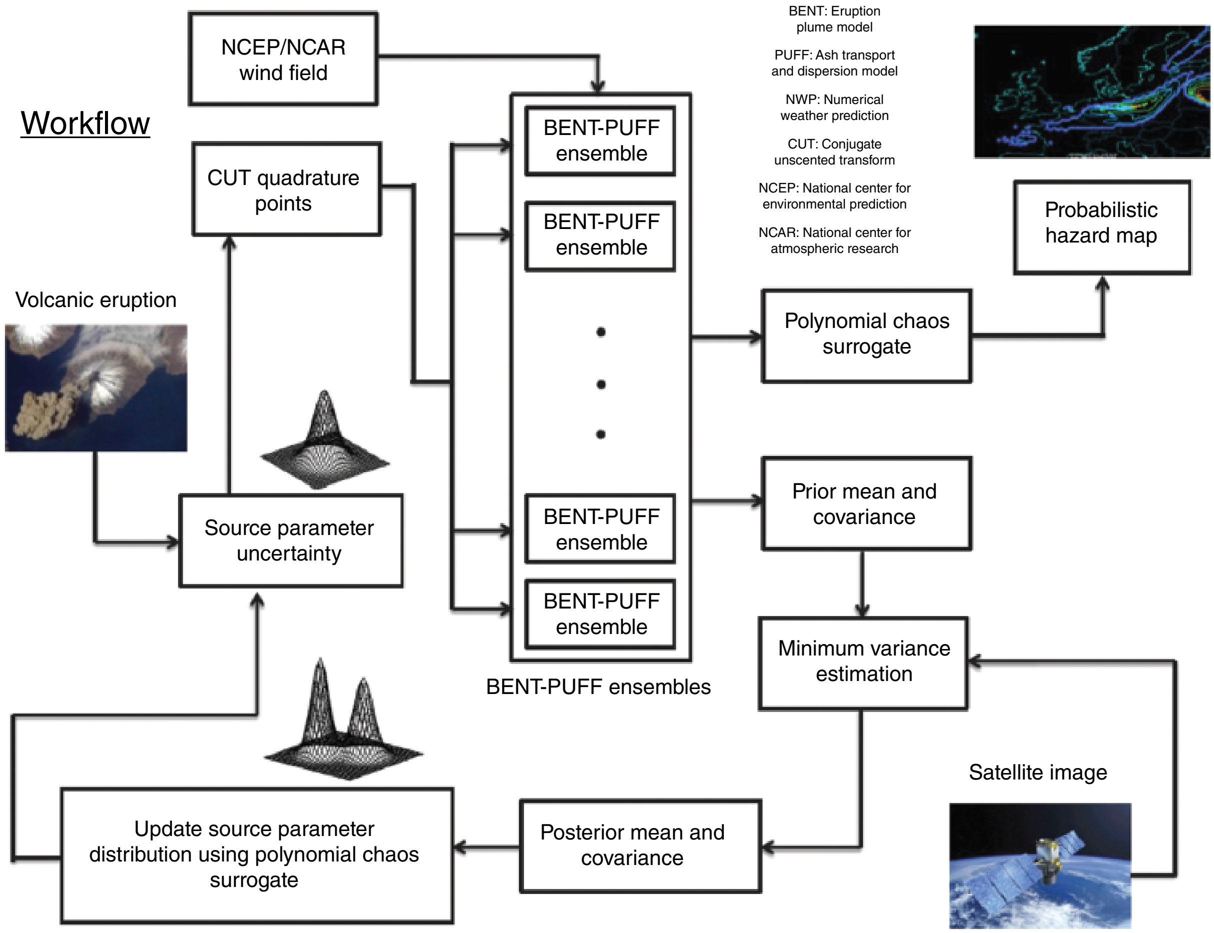

Figure 6.2 Probabilistic modeling workflow, adapted from *Madankan et al.* [2014], using the Puff VATD model and coupled one-dimensional plume rise model, BENT.

uncertainty in the eruption source input. We have chosen the vent radius (m), vent velocity (m/s), log mean grain size (μm), and standard deviation of log grain size. Given the local radiosonde and the range of these four values along with the BENT model results, we end up with 161 different sets of source parameter inputs for the Puff VATD model. Each has a specific likelihood of occurrence based on the volcano's physical characteristics (vent size and velocity) and previous eruption style (mean ash grain size and standard deviation of distribution). This can be adapted to any volcano of interest. The BENT model within Puffin provides the maximum plume altitude (km), vertical plume shape, initial grain-size distribution for dispersal, and mass eruption rate (MER, kg/s). We specify the event length to convert the MER to total erupted mass (kg). Several Puffin simulations can run in parallel to reduce the time to complete the full suite of simulations. For example, with two Puff simulations running in parallel, each with a dedicated processing node and 1e5 (100,000) ash particles, the wall-clock time for the 161 simulations was 2.4 hr (approx. 1.8 min per simulation pair) on a 23 CPU-node server and using approximately 100 MB of allocated memory.

The processing routines will run the Puffin tool for each of the 161 simulations to generate the Puff input file. As each parallel run completes, the Puff particle location and ash-concentration output files are generated and the routines moves down the list of the 161 simulation members. In the final part of the NRT processing routines, the outputs from the simulations are generated using the initial weightings defined in for the source parameters to generate a mean ash concentration. These results are sent to the second postprocessing routine to produce the probabilistic maps as GEOTIFF data, JPEG imagery, and Google Earth KML and KMZ files.

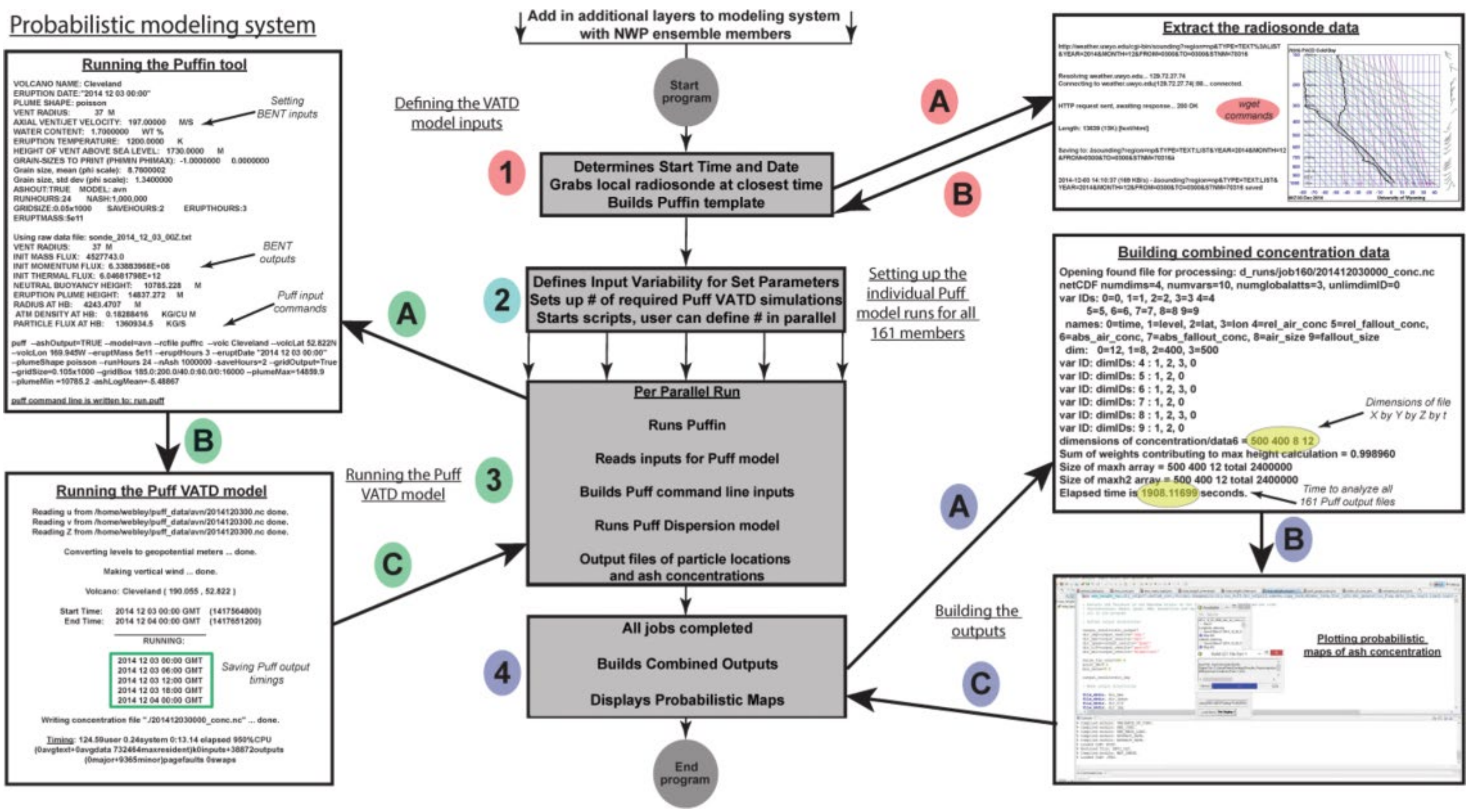

Figure 6.3 Real-time processing routines from the probabilistic modeling of volcanic ash clouds. Results from these routines include mean ash mass loadings and ash concentrations at defined altitudes from all 161 ensemble members.

6.3. PROBABILISTIC MODELING RESULTS

6.3.1. Cleveland Volcano, Alaska, USA: 3 December 2014

Cleveland volcano was at elevated alert during early December 2014 [*AVO*, 2014] so we set up probabilistic model simulations to assess the capability of the system to develop timely results and to assess if improvements were needed in our workflow for future eruptions. The volcano did not erupt but our example illustrates how the system could provide pre-event warnings to assist in VAA and VAG generation for aviation safety. The Puffin tool determined plume top heights to range from 12.2 km to 18.95 km above sea level (ASL) and mean particle size to range from 2.3 to 3.7 μm. Figure 6.4 shows output from one Puff model simulation (i.e., Simulation Number 1). For this simulation, Puffin determined the plume top height to be 14.6 km ASL, the mean particle size to be 3 μm, and the total mass to be 5×10^{11} kg. For this and all the Puff model simulations, we used the North American model (NAM) 216 grid at 45 km spatial resolution to provide the atmospheric data for the simulations.

Figure 6.4 displays the two outputs available from the Puff VATD model. Being Lagrangian in form, the particle locations in four dimensions (x, y, z, and t), along with the ash concentrations (g/m^3) can be generated per time step. The volcanic-ash mass loadings (g/m^2) are derived as total atmospheric column loadings from the ash-concentration gridded data. Figure 6.4 shows the ash locations and mass loadings at + 12 hr into the simulation, or 12:00 UTC on 3 December 2014. There is evidence of fallout close to the volcano with a highest mass loading of 40.5 mg/m^2.

The next step in our routine is to combine the 161 model simulations together. Figures 6.5, 6.6, and 6.7 document the averaged mass loadings and concentrations from all the simulation members along with the probabilities associated with exceeding specific mass and concentration thresholds. For the averaged results, the location of the cloud closely matches that from Simulation Number 1 (Fig. 6.4), while the concentrations at 2 km, 10 km, and 16 km ASL illustrate the different footprints predicted by the Puff model as a result of the variations in wind patterns at these altitudes. The highest altitude portion, 16 km ASL, is centered in the westerly section of the cloud, and the lower altitude portions, below 10 km ASL, are focused in the easterly and southeasterly sections. Figure 6.5a documents the ash-mass loading from the averaged results of the 161 simulations. Figure 6.5b shows that there is little variability in the 161 members and that the uncertainties in the model inputs led to a (spatially) well-constrained set of simulations. Figure 6.5a and Figure 6.5b together illustrate that mass loadings greater than 0.1 mg/m^2 correlate to the location of the higher probabilities of ash presence.

Figure 6.6a shows the mean concentrations from all 161 members at 2 km ASL, while Figure 6.7a shows the corresponding probabilities of the concentration $> 1 \times 10^{-6}$ g/m^3 (=1μg/m^3) our chosen ash versus no-ash boundary. Figure 6.7a produces a very conservative representation of ash-cloud location. The 2010 eruption of Eyjafjallajökull volcano [*Gudmundsson et al.*, 2010] showed the impact of how the ash-cloud "edge" is defined in model data where the modeled cloud extent was much greater than seen in the satellite data. Our conservative no-ash versus ash boundary at 1μg/m^3 is a factor of 1000 lower than the 1–4 mg/m^3 proposed during the Eyja events. Satellite observations would be needed to compare to our probability of occurrence to generate posterior model inputs for an improved simulation and asses our chosen no-ash versus ash boundary threshold.

Figures 6.6b and 6.7b show the mean ash concentrations and probabilities of ash occurrence $\geq 1 \times 10^{-6}$ g/m^3 at 10 km ASL, while Figures 6.6c and 6.7c show the same parameters at 16 km ASL. The results at 16 km ASL show that some of the simulations have a smaller spatial footprint. Figure 6.7c shows that the region of 100% probability of concentrations exceeding 1×10^{-6} g/m^3 is confined to the northwest segment of the cloud footprint matching the higher concentrations from the 161 members (Fig. 6.6c). Significantly reducing the concentration threshold to 1×10^{-12} g/m^3 would result in the cloud footprints at 2 km, 10 km, and 16 km ASL being almost identical.

6.3.2. Zhupanovsky Volcano, Kamchatka, Russia: 29 December 2014

GVP [2015] reported that Zhupanovsky volcano had continuing activity leading to an eruption with a plume top height of 6–9 km ASL on 29 December 2014. For our probabilistic modeling, we set a start time of 00:00 UTC. The Puffin tool determined the plume heights ranged from 10.7 to 13.3 km ASL and the mean size from 2.3 to 3.7 μm across our 161 simulation members. Here we used the NCEP Global Forecast Systems (GFS) 1.25° spatial resolution NWP data with the Puff VATD model. Figure 6.8 illustrates the results for Simulation Number 1 from the Zhupanovsky event with the particle locations and ash-mass loadings presented at + 12 hr after the event start. There is evidence of ashfall close to the volcano in the particle location output while the highest mass loadings occur in the eastern extent of the dispersing cloud. For this simulation, the plume top height was 11.2 km ASL with a mean particle size of 3.2 μm and at +12 hr into the simulation the maximum mass loadings was 5.6 mg/m^2.

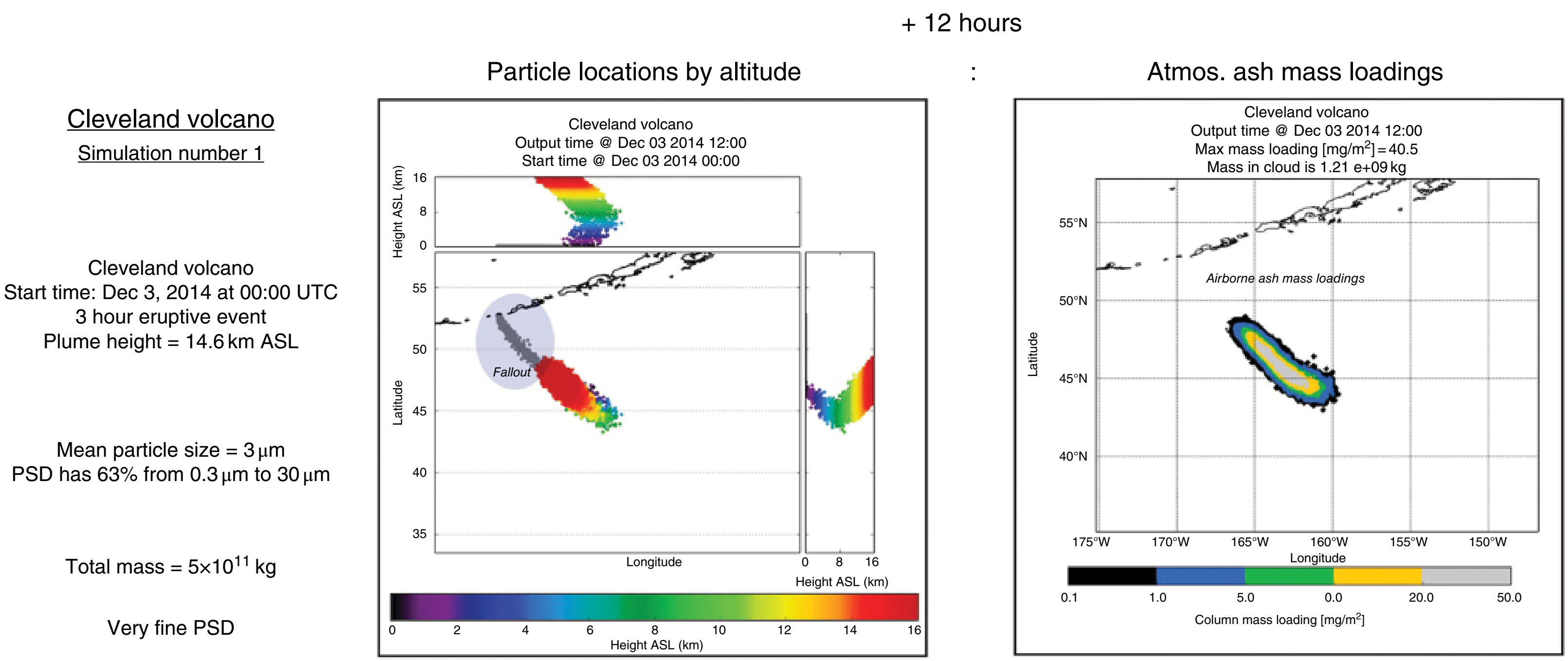

Figure 6.4 Cleveland Volcano Puff VATD model simulation for Probabilistic Simulation number 1. This is for start time on 3 December 2014 at 00:00 UTC with the particle locations and ash mass loading (mg/m^2) at + 12 hr after the eruption start, or 12:00 UTC.

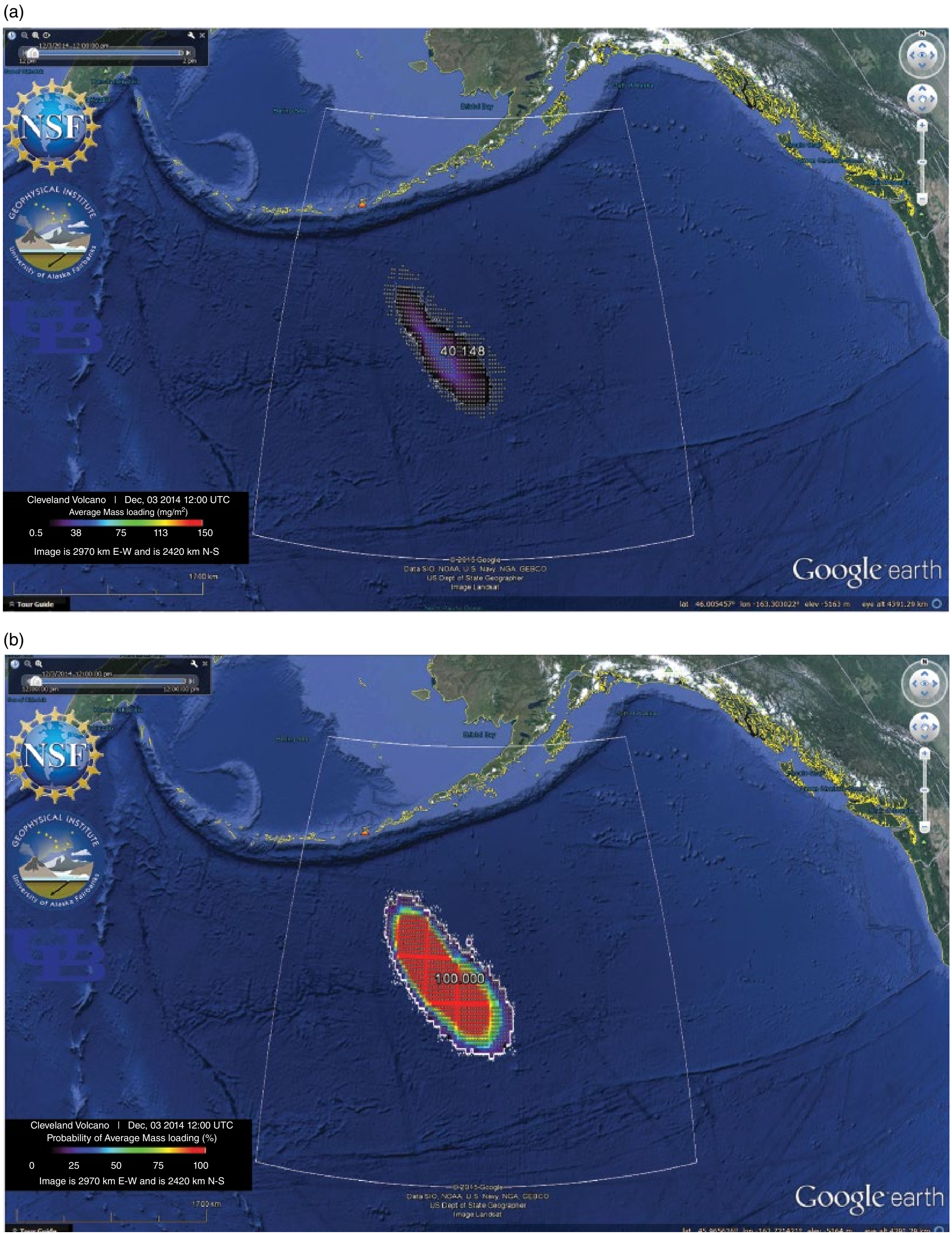

Figure 6.5 Probabilistic modeling outputs at 12:00 UTC, + 12 hr after eruption, for Cleveland 3 December 2014 model simulation. (a) Mean of the 161 simulation members showing ash mass loadings (mg/m^2) and (b) probabilities (%) of ash mass loading exceeding predefined threshold.

(a)

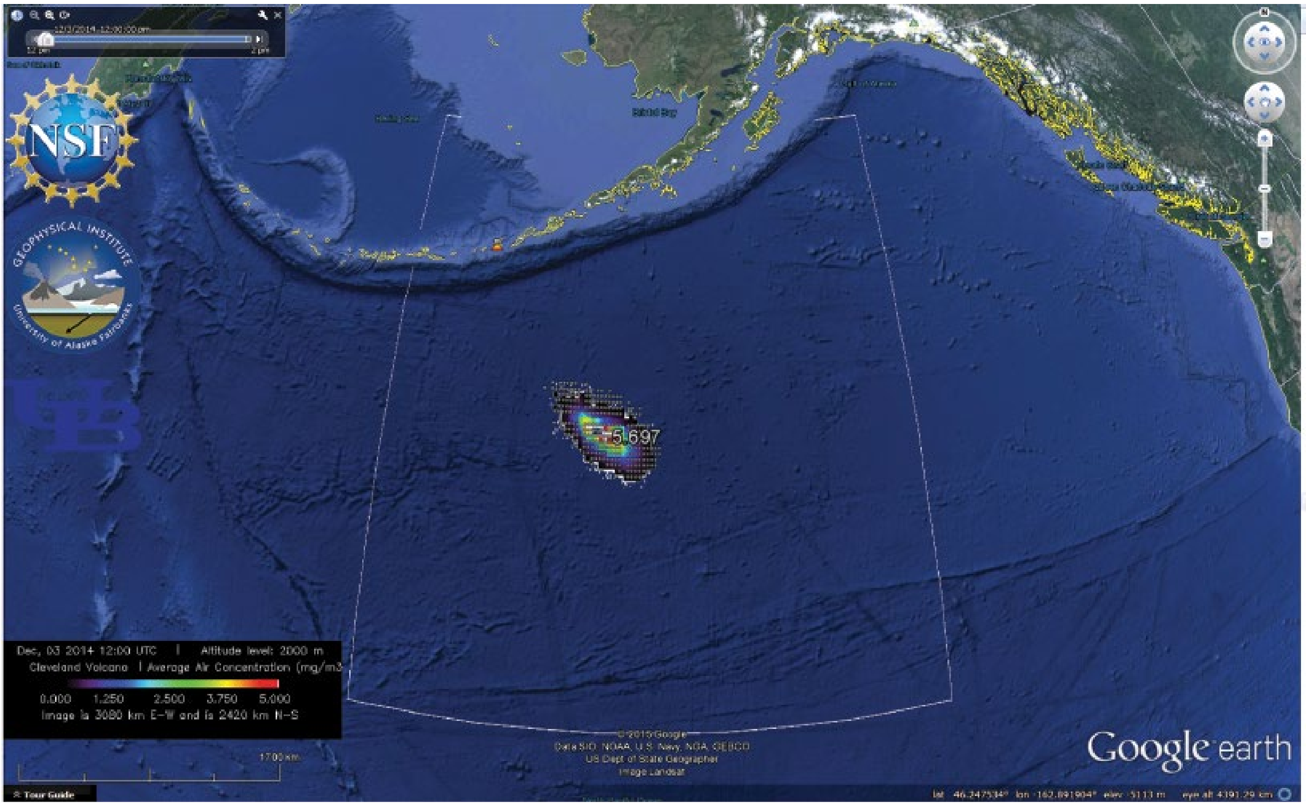

(b)

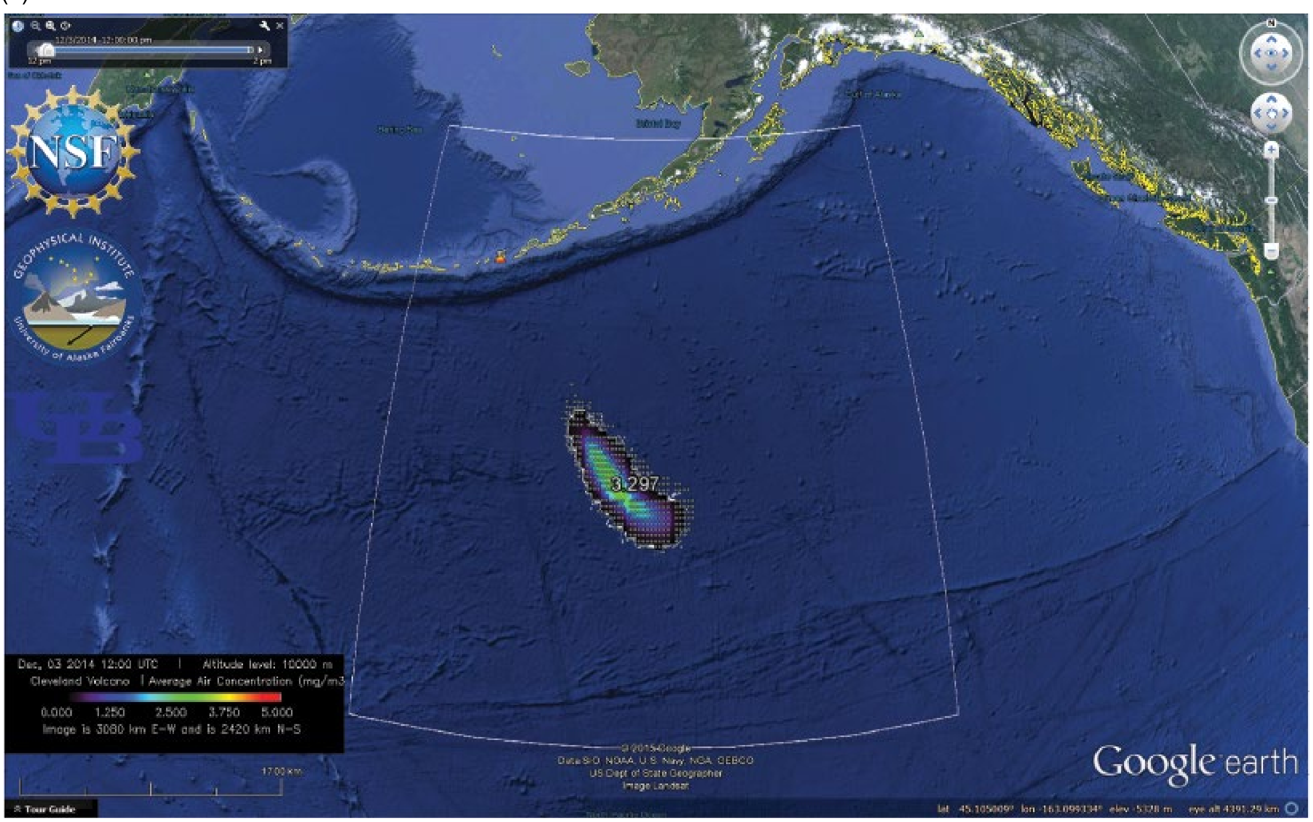

Figure 6.6 Probabilistic modeling outputs at 12:00 UTC, + 12 hr after eruption, for Cleveland 3 December 2014 model simulation. Mean results from the 161 simulation members showing ash concentrations (mg/m^3) at 2 (a), 10 (b), and 16 (c) km ASL.

(c)

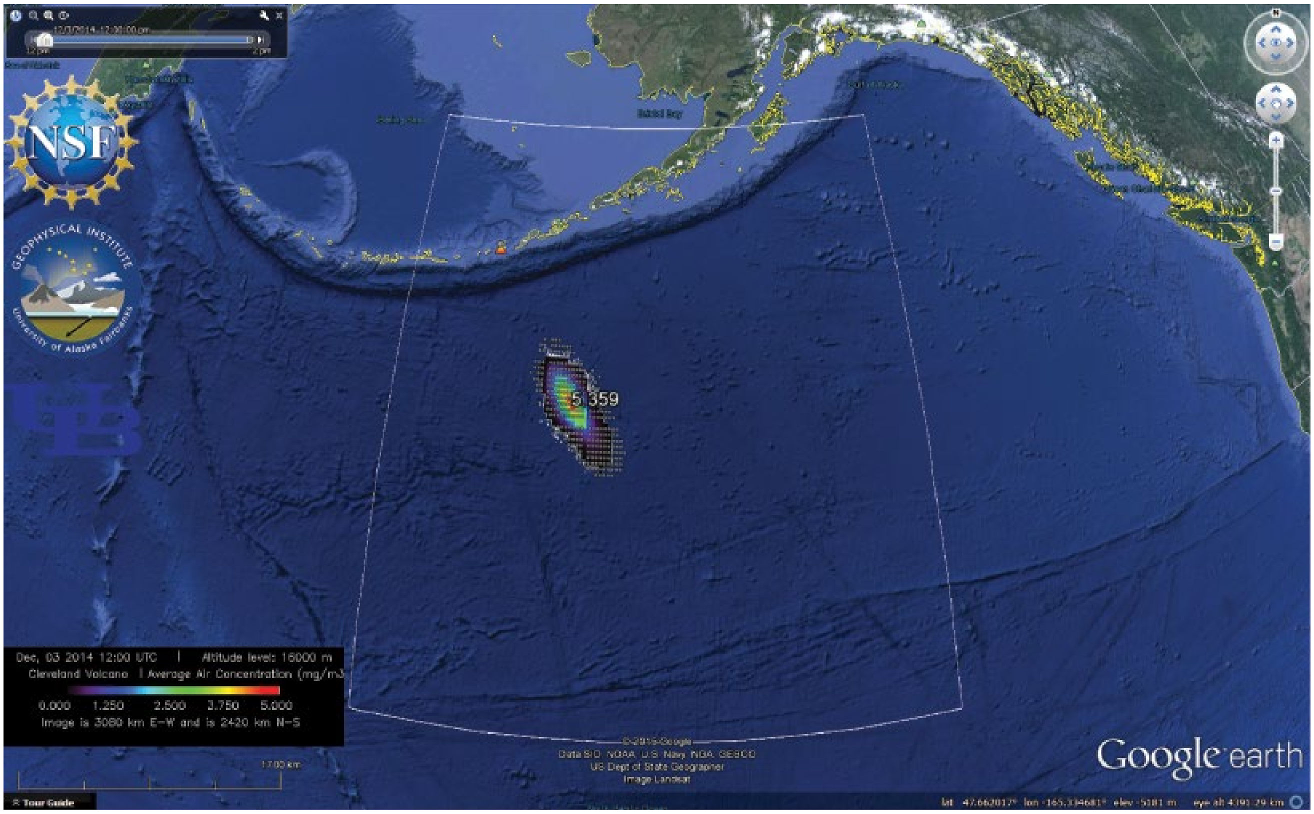

Figure 6.6 (Continued)

6.3.2.1. Comparison of the Mean and Probabilities of All Simulations

Figure 6.8 illustrates a problem in using predefined grids for the ash-concentration data. The particle location map is defined by the maximum extent of the ash particles in the 24 hr period while the concentration grid is set prior to the simulation. Therefore, the cloud could disperse beyond the extensions of the concentration grid. Further developments are needed to our approach to define the concentration grid domain at the end of the simulation rather than as a predefined domain. Puff simulates the ash-particle dispersal and generates a final concentration grid. We can predefine this grid with a fine spatial resolution and a large domain to cover the maximum possible extent of the cloud dispersal in 24 hr. This would generate large (> 4 GB) gridded datasets that are not optimal in terms of file size and spatial resolution for operational data analysis. Running the model simulations with a small number of ash particles would allow us to evaluate the maximum extent of the ash cloud to then optimally design the concentration grid to capture the full cloud dispersal and set the finest possible spatial resolution. However, to implement this for our model simulations is beyond the scope of the research shown in this chapter. Figure 6.9 shows the results of the probabilistic modeling for the 29 December simulations from Zhupanovsky volcano at + 12 hr after the start of the event. Figure 6.9b shows the ash-loading probabilities where concentrations exceeded 10^{-6} g/m^3 or 1 μg/m^3. Further examples can be seen in Figures 6.10 and 6.11 for ash concentrations and their probabilities at 2 km, 6 km, and 10 km ASL.

For Zhupanovsky volcano, we also illustrate the significance of the minimum threshold chosen for the probabilistic analysis and how it could impact the spatial footprint applied in developing a VAA. Figure 6.12 shows the probabilities of measureable ash-mass loadings for six different minimum exceedance thresholds for the concentration data at +12 hr into the simulations. None of the 161 members forecasted a concentration ≥ 100 mg/m^3 (Fig. 6.12a). Moving from exceedance thresholds ≥ 10 mg/m^3 (Fig. 6.12b) to ≥ 0.1 mg/m^3 (Fig. 6.12e) there is evidence of a growing cloud footprint and in the region of 100% probability of exceeding the threshold. As we

(a)

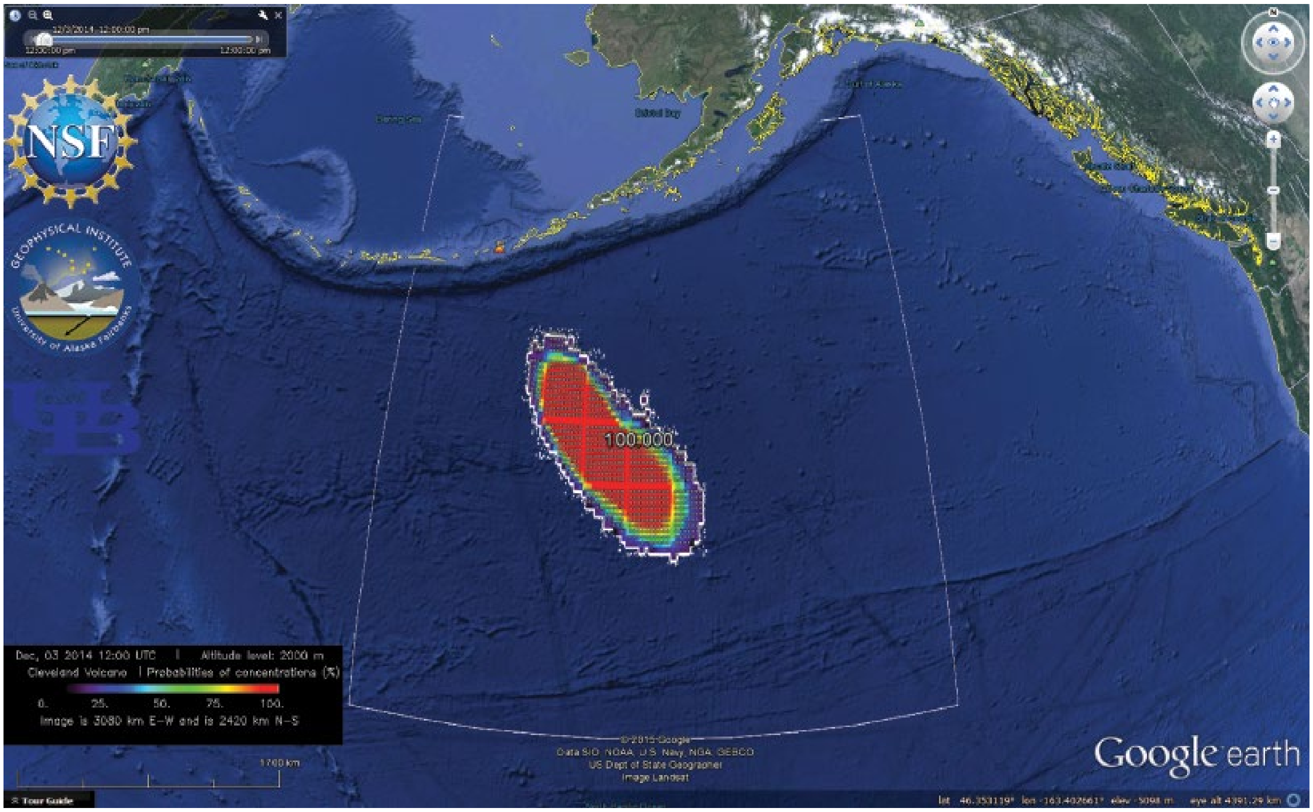

(b)

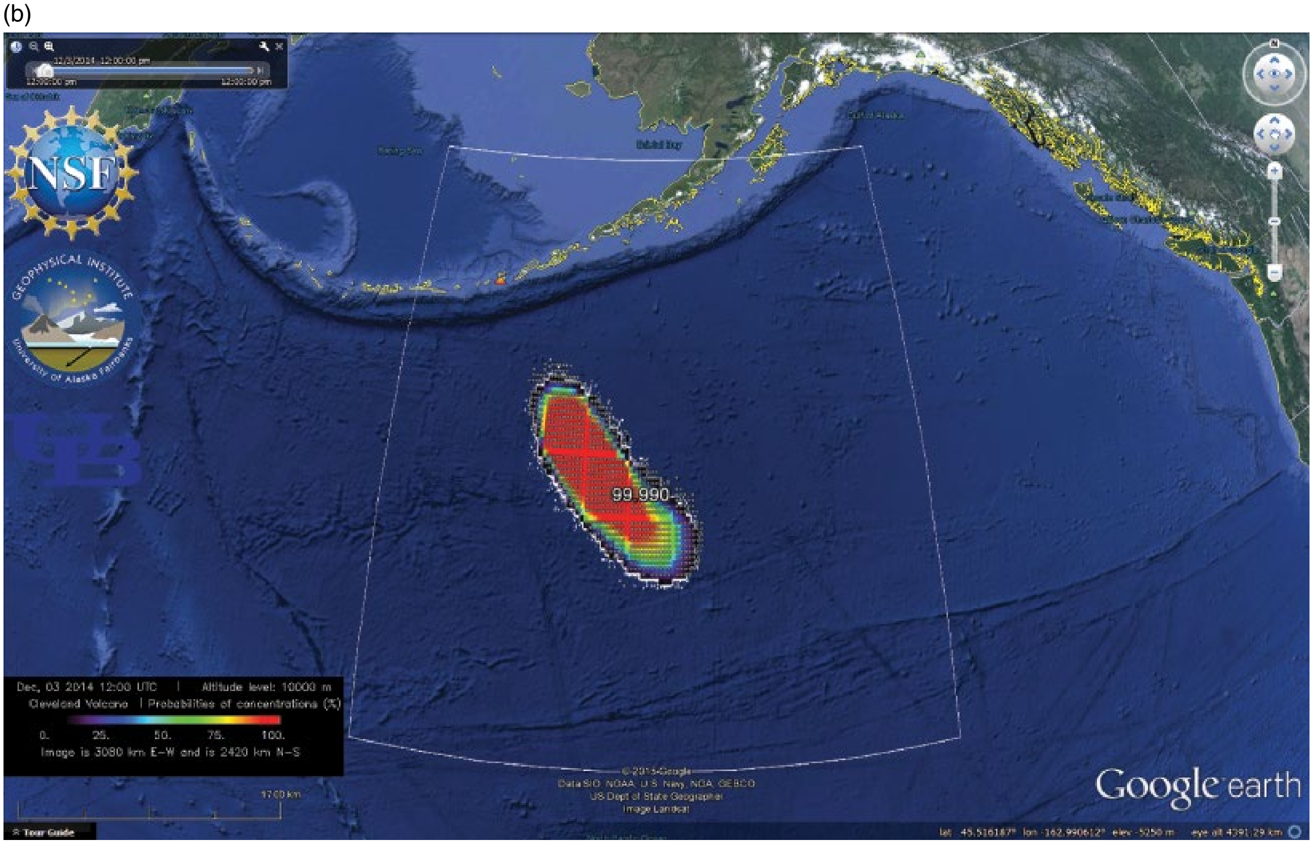

Figure 6.7 Probabilistic modeling outputs at 12:00 UTC, + 12 hr after eruption, for the Cleveland 3 December 2014 model simulation. Probabilities (%) of ash concentration (mg/m^3) exceedances at 2 (a), 10 (b), and 16 (c) km ASL.

(c)

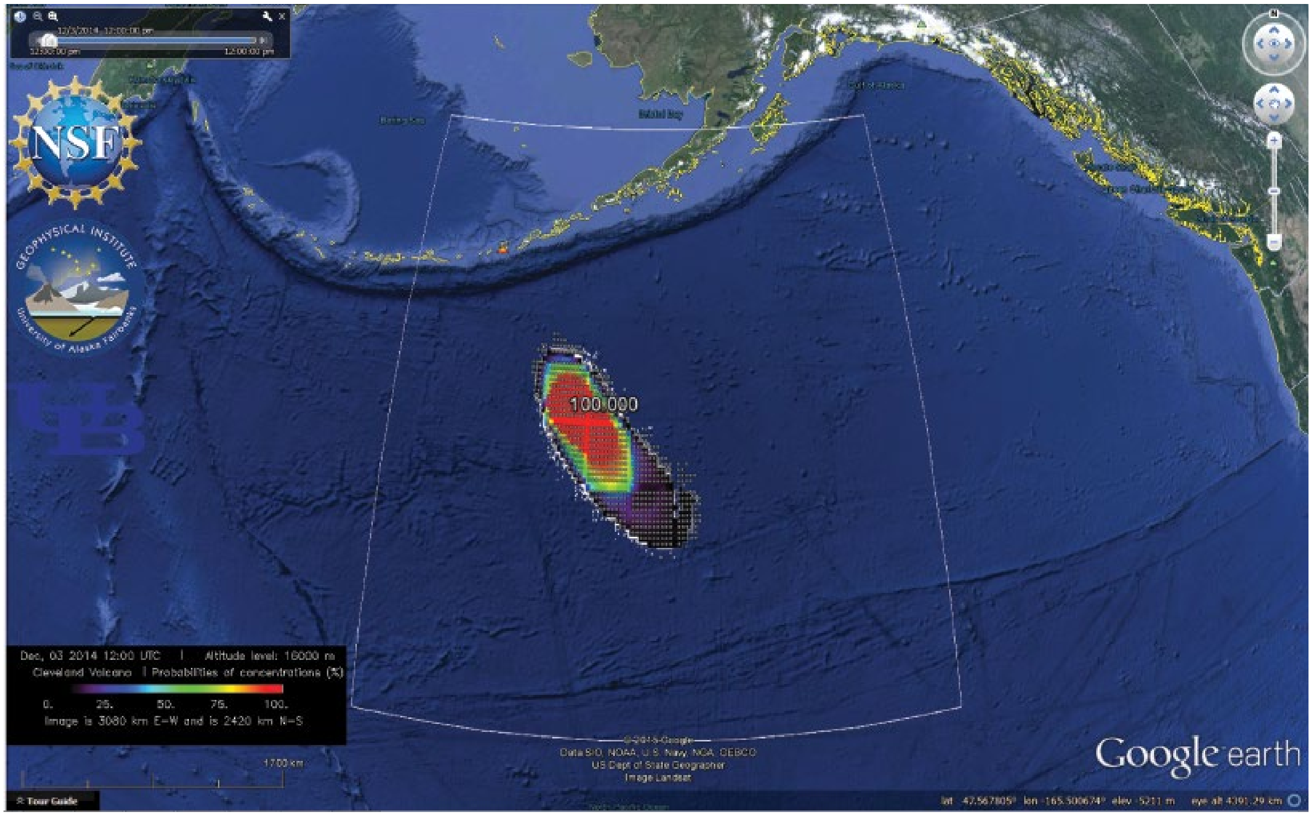

Figure 6.7 (Continued)

reduce the constraints on the minimum concentration threshold, the probability of a measureable ash-mass loading increases.

By examining the probabilities of exceeding specific concentrations, there is evidence of significant differences at varying altitudes in the atmosphere. For the probabilities at 2 km ASL, the spatial footprint is similar to that from the mass loadings (Fig. 6.12). Comparing the probabilities at 2 km ASL (Fig. 6.13) to 10 km ASL (Fig. 6.14), significant differences occur. For a concentration threshold of 100 mg/m^3, there was no probability of exceedance in the gridded concentration at either 2 km ASL (Fig. 6.13a) or at 10 km ASL (Fig. 6.14a). By relaxing the concentration threshold by a factor of 10, Figure 6.13b–f for 2 km ASL and Figure 6.14b–f for 10 km ASL illustrate an increasing spatial extent to the simulated cloud occurs.

Our results show that the probability of exceeding the same specific concentration threshold varies significantly by altitude. Awareness of this vertical variability is critical for those in real-time hazard assessment where there is a need to produce maps at critical altitudes or flight levels for the aviation industry. Figures 6.15 and 6.16 show how the spatial extent of the probabilities varies with time for differing concentration thresholds. Here we fix the altitude to only compare concentration probabilities at 2 km ASL or the lowest vertical level of the Puff VATD model outputs. As the cloud grows in size, the spatial extent of the probability of the defined thresholds being exceeded also grows directly correlated to the level of cloud dispersal as simulated by Puff.

6.3.2.2. Comparing Individual Members and the Mean of All Simulations

There is a need to compare individual simulation members to the mean of all simulations as well as compare the probabilistic results to any observational data. Then the probabilistic modeling approach can be elevated to determine if it provides more information on the potential variability in the ash-cloud dispersion and is useful for operational hazard assessment. For the Zhupanovsky simulation, rather than examine all 161 members and compare them one by one to each other and the mean results, we compared simulation members numbered 51 and 160. These two members represent the Puff model runs with the maximum and minimum initial

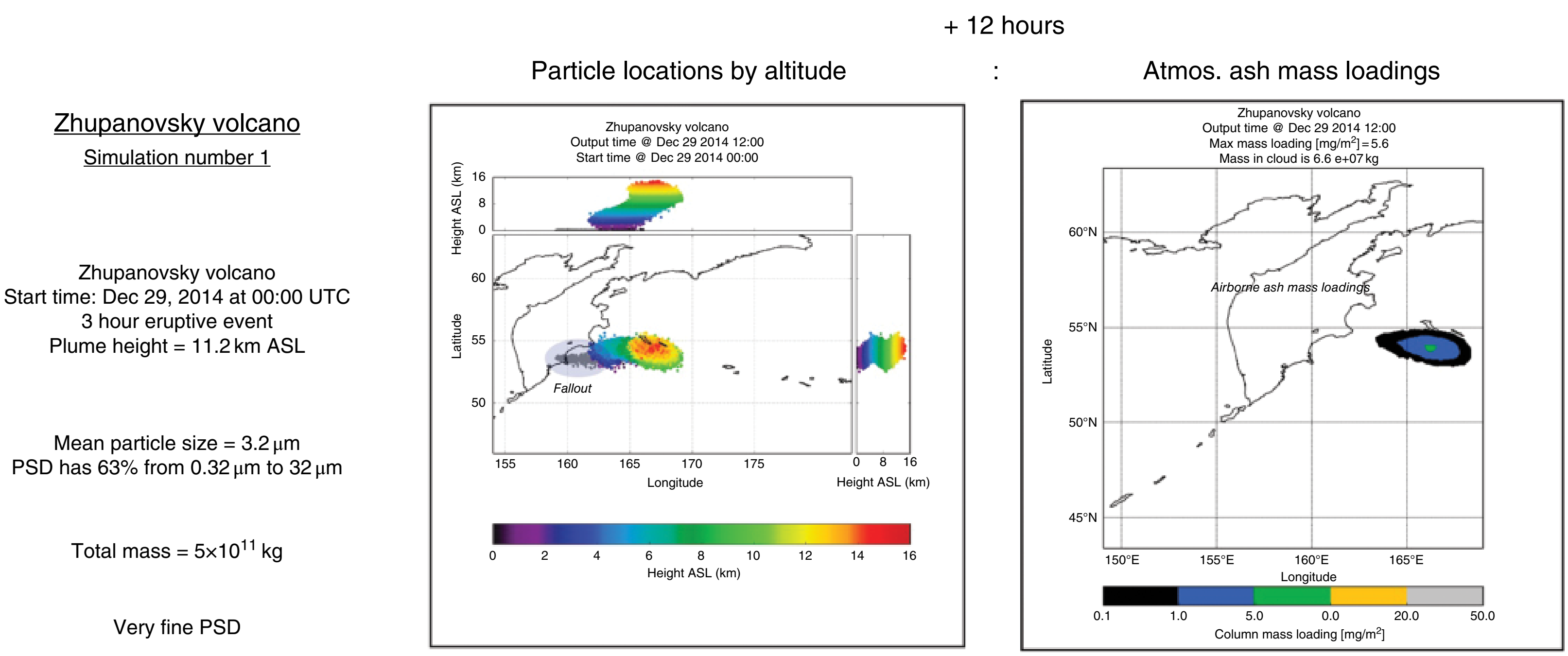

Figure 6.8 Zhupanovsky Volcano Puff VATD model simulation for probabilistic run number 1. This is for start time on 29 December 2014 at 00:00 UTC with the particle locations and ash mass loading (mg/m^2) at + 12 hr after the eruption start, or 12:00 UTC.

(a)

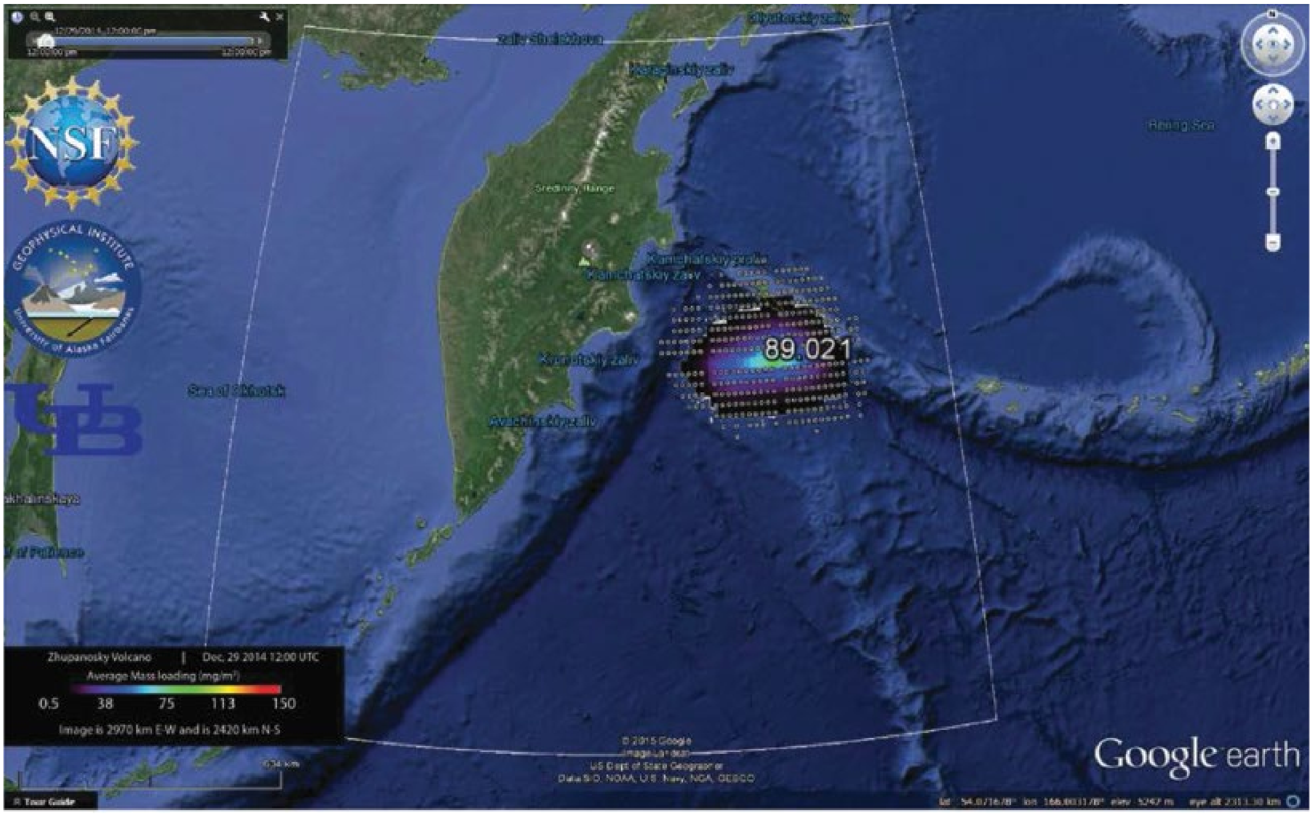

(b)

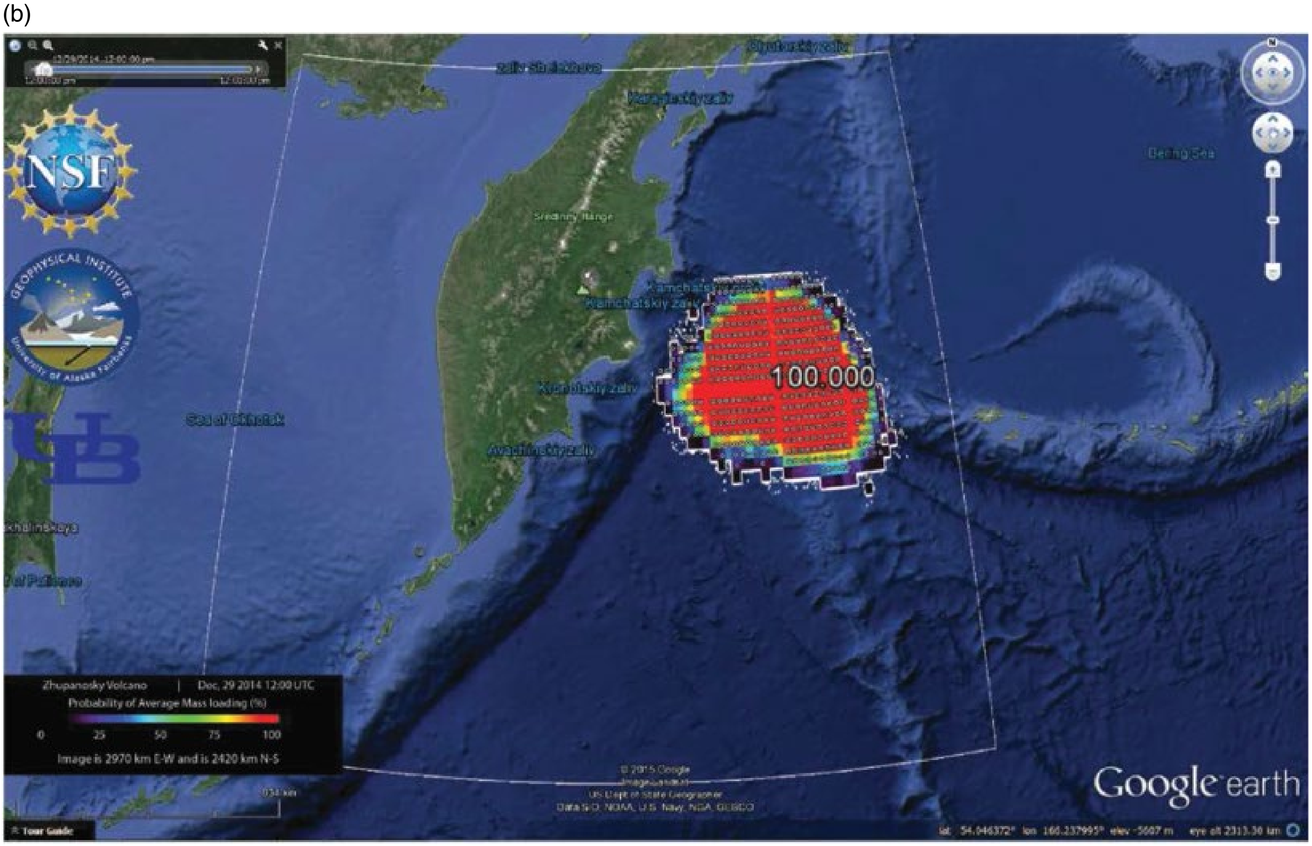

Figure 6.9 Probabilistic modeling outputs at 12:00 UTC, + 12 hr after eruption, for Zhupanovsky 29 December 2014 model simulation. (a) Mean of the 161 simulation members showing ash mass loadings (mg/m²) and (b) probabilities (%) of ash mass loading exceeding predefined threshold.

(a)

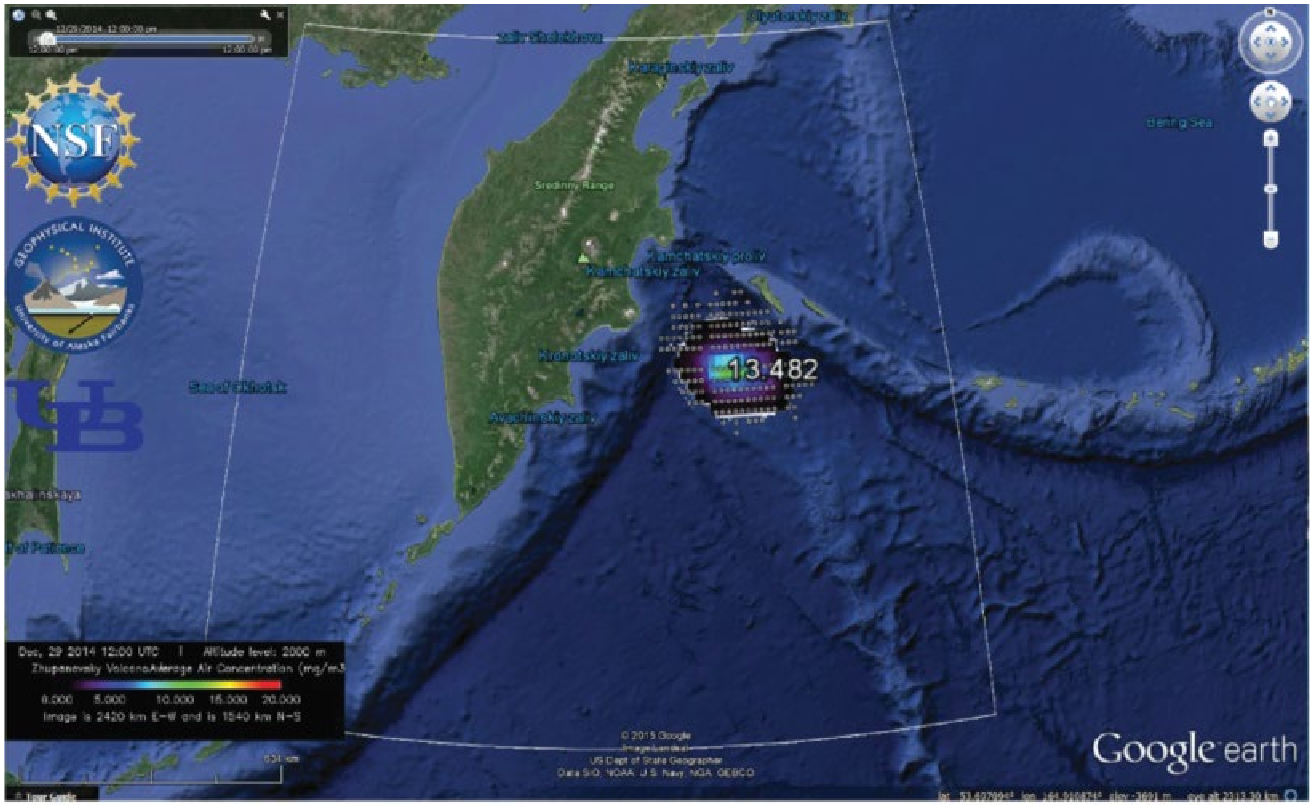

(b)

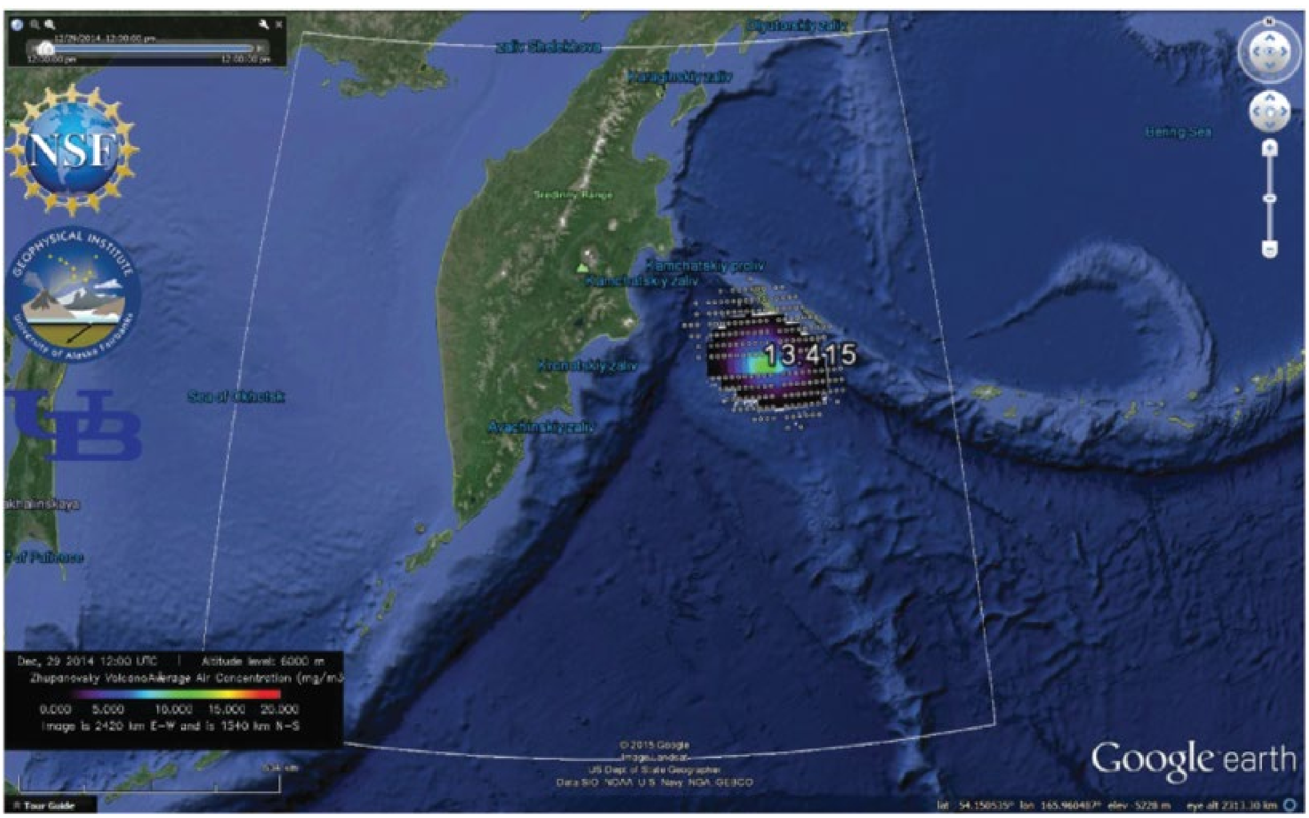

Figure 6.10 Probabilistic modeling outputs at 12:00 UTC, + 12 hr after eruption, for Zhupanovsky 29 December 2014 model simulation. Mean results from the 161 simulation members showing ash concentrations (mg/m^3) at 2 (a), 10 (b), and 16 (c) km ASL.

(c)

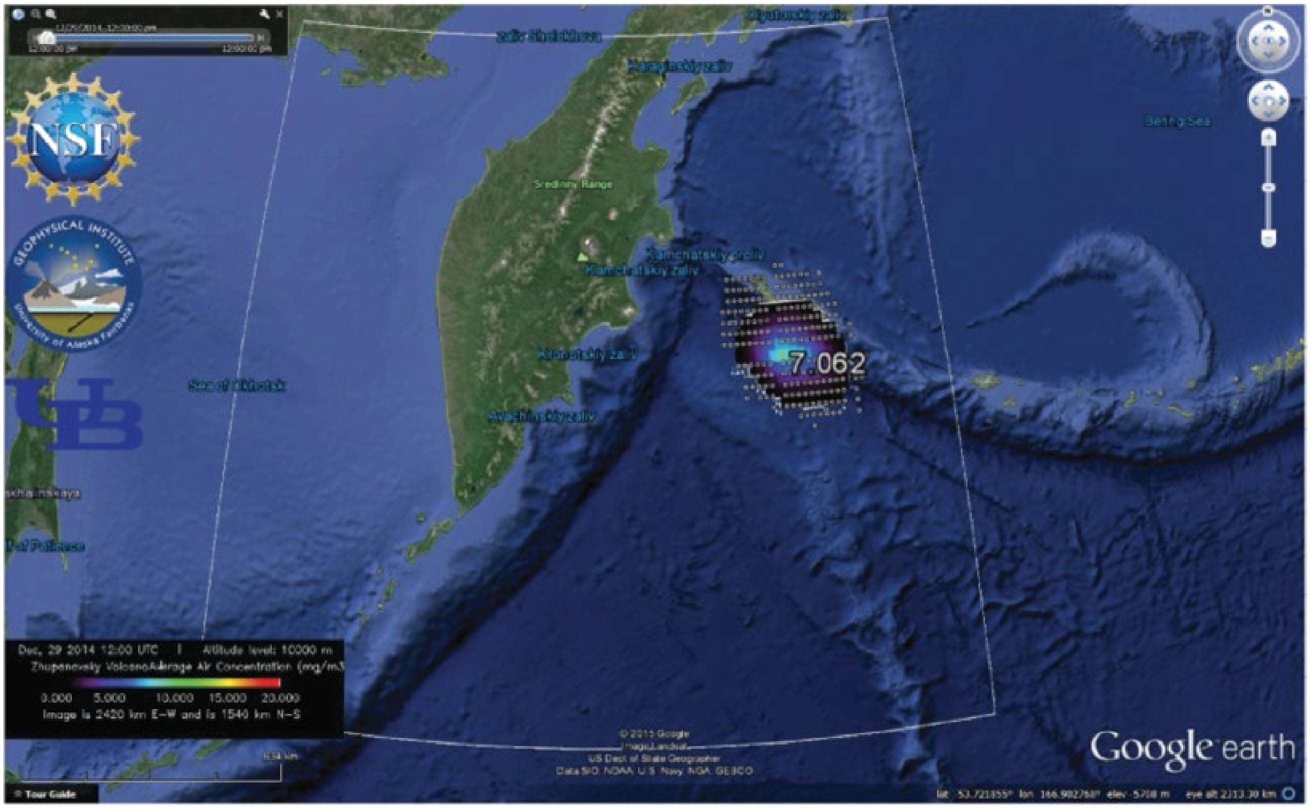

Figure 6.10 (Continued)

plume heights, 10.98 km ASL for Run Number 51 and 13.63 km ASL for Run Number 160. Each model simulations used the same initial vertical shape (Poisson distribution to represent an umbrella-shaped cloud) while the PSD was defined directly from the Puffin model. For Simulation Number 51, Figure 6.17a shows the Puff particle locations in plan view along with longitudinal and latitudinal cross sections. Figure 6.17b shows the mass loadings with a polygon defining the spatial extent for all locations where mass loadings exceed 1 mg/m^2. Figure 6.17c shows the ash concentrations at 10–12 km ASL with its associated polygon for concentrations exceeding 1 mg/m^3.

These can be directly compared to the corresponding results from Simulation Number 160 : Figure 6.17d for particle locations, Figure 6.17e for mass loadings, and Figure 6.17f for ash concentrations. The higher altitude initial plume for Simulation Number 160 has an impact on the footprint of the mass loadings and ash concentrations. This is highlighted in Figure 6.18, which compares the polygons for mass loadings and 10–12 km ASL concentrations to the mean of the 161 simulations. Figure 6.18a, for the mass loadings, shows small differences in the total footprints (Number 51 at 44,500 km^2, Number 160 at 47,500 km^2, and the mean of all the runs at 54,000 km^2). The impact of the higher initial plume height in Run Number 160 is seen to greater effect in the area of the ash concentrations at 10–12 km ASL (Number 51 at 16,600 km^2, Number 160 at 26,300 km^2, and the mean of all the runs at 32,700 km^2). Here, the Simulation Number 160 (Fig. 6.18b) extends farther to the northwest as compared with Simulation Number 51. As the cloud disperses, this displacement between the two runs grows with time.

6.4. DISCUSSION

Our results show how probabilistic modeling can be used to assess the probability of exceeding a ash concentration and/or mass loading threshold in both space and time. The higher the probability, the more likely this threshold would be exceeded. This can provide a higher degree of confidence in the modeling results and be used to build a map of the area most at risk to concentrations/mass loadings greater than the specific threshold. Figures 6.5 to 6.7 for Cleveland volcano and Figures 6.9

(a)

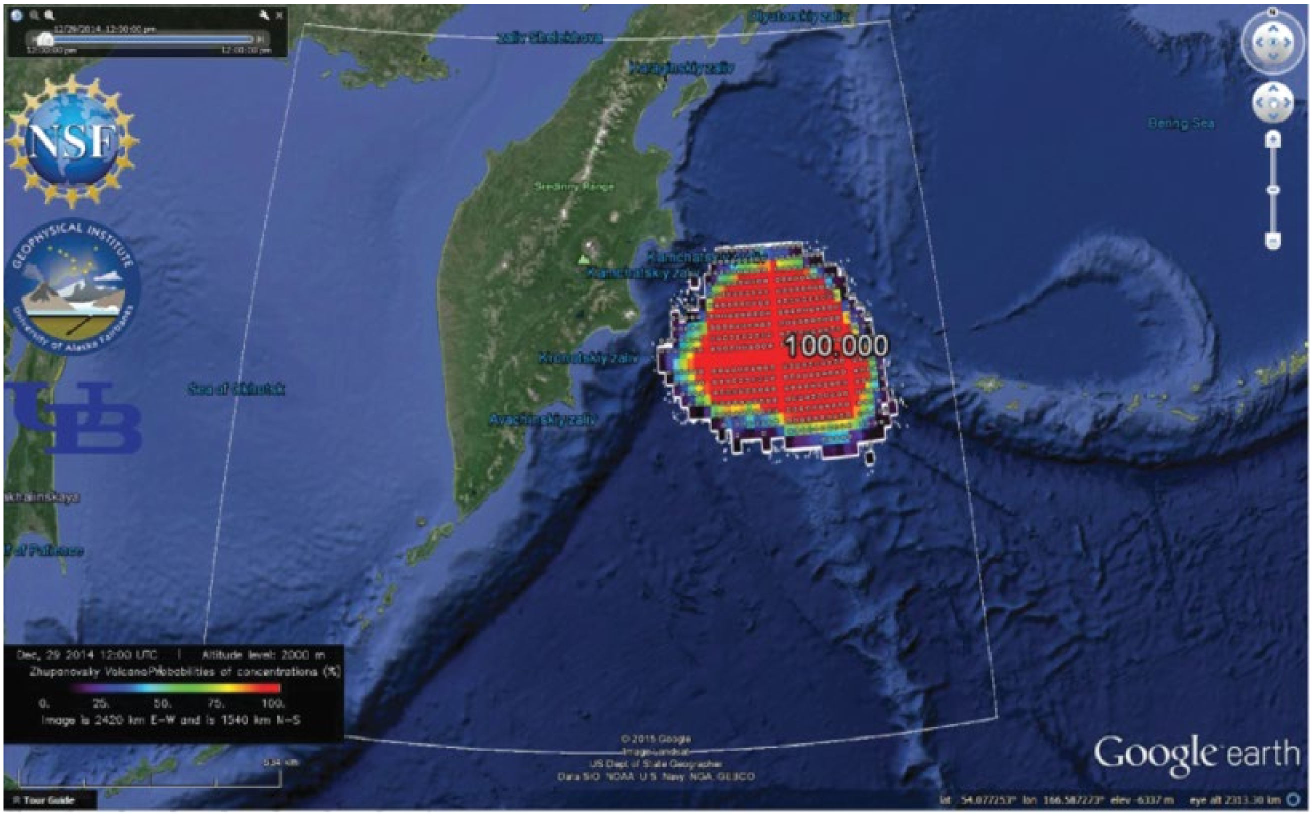

(b)

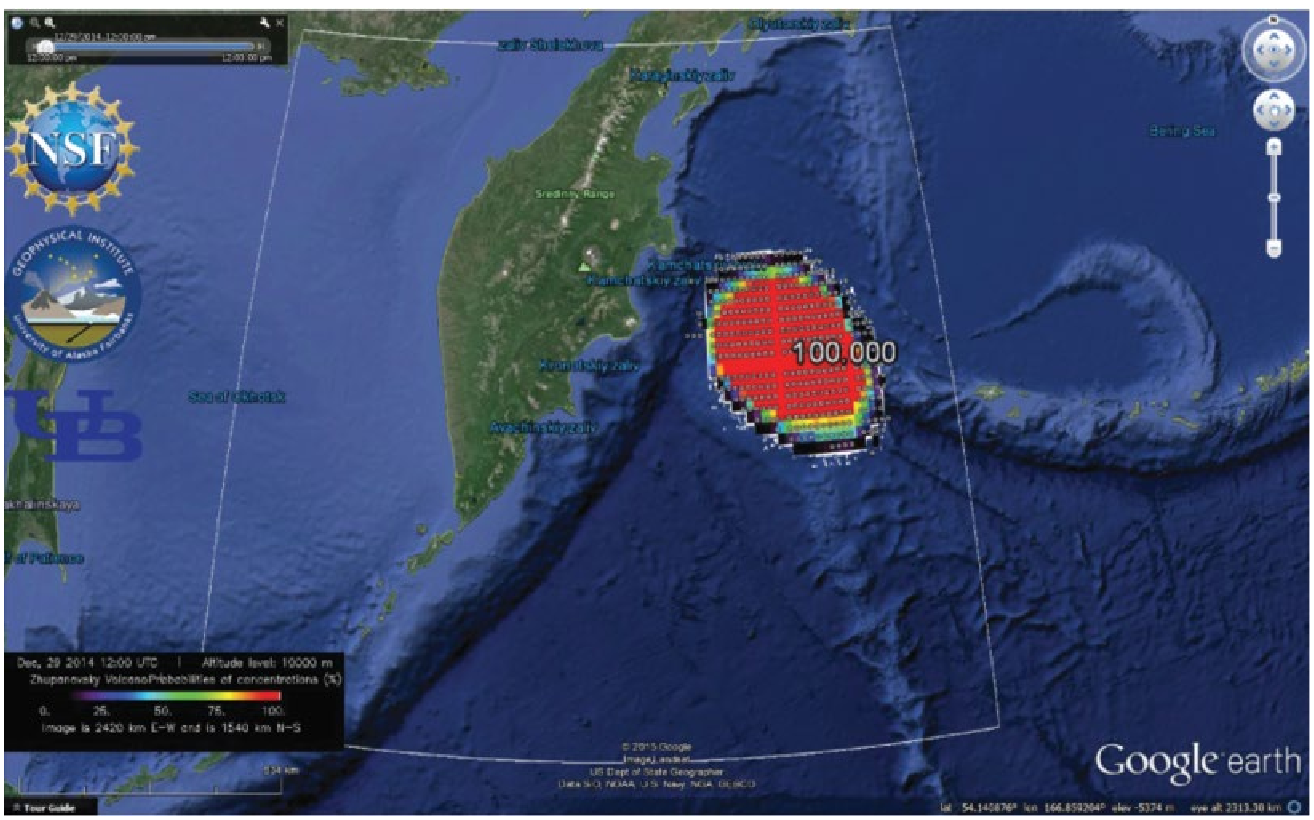

Figure 6.11 Probabilistic modeling outputs at 12:00 UTC, + 12 hr after eruption, for Zhupanovsky 29 December 2014 model simulation. Probabilities (%) of ash concentration (mg/m^3) exceedances at 2 (a), 10 (b), and 16 (c) km ASL.

(c)

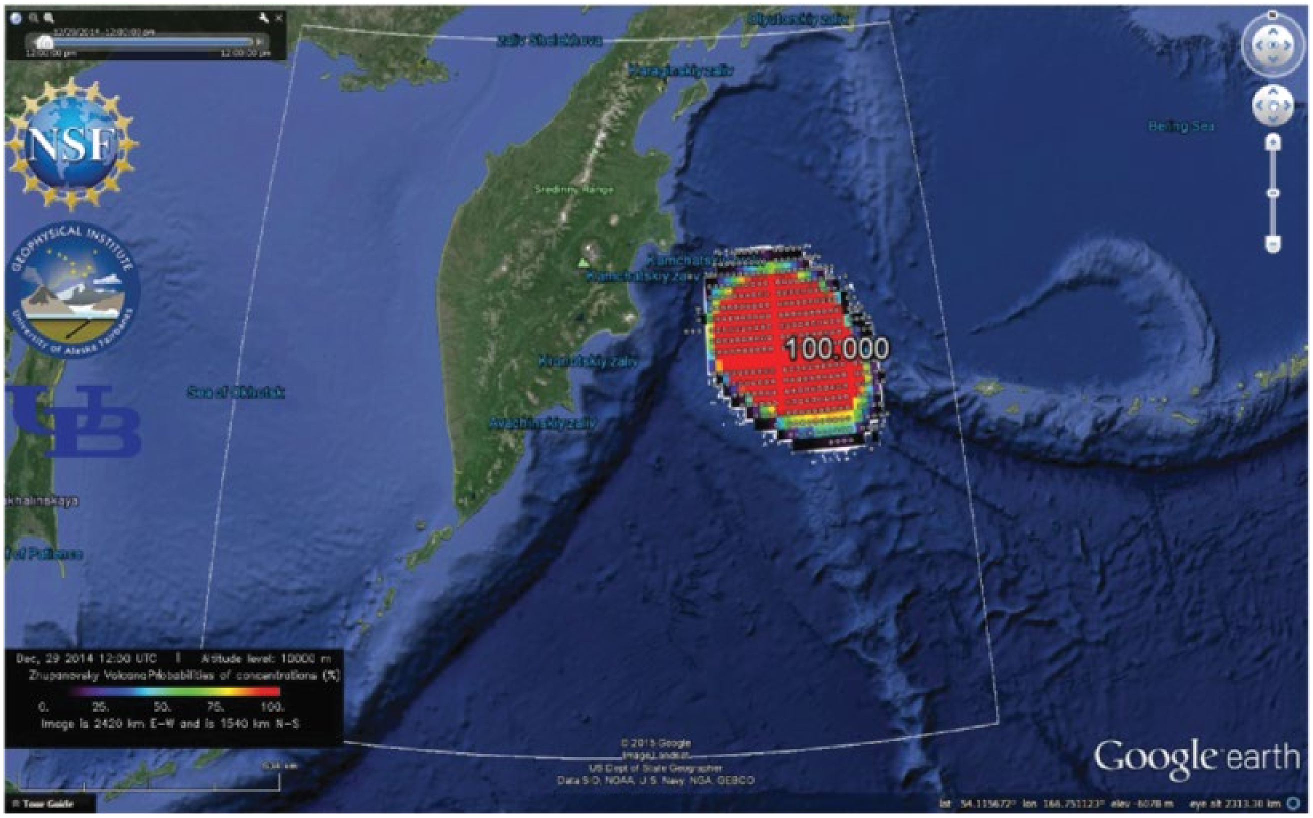

Figure 6.11 (Continued)

to 6.16 for Zhupanovsky volcano show outputs from our probabilistic modeling workflow. For real-time assessments of the ash-cloud impact and likely location and concentration, the communication of our and any available probabilistic results to the end user becomes critical. Displaying the results in a common interface and ensuring they are compatible with tools currently used to generate VAA and VAG should be a focus of researchers and operational organizations developing the probabilistic modeling capabilities.

For our contribution to the monograph, we focused on four eruption source inputs to the VATD modeling of the cloud. Observational data are needed to constrain the results from any dispersion modeling and update prior knowledge of the input parameters and associated uncertainties into posterior input data for updated VATD model simulations. Prior to an eruption, the likely maximum, minimum, and mean/median value for the modeling input parameters can be chosen. Several questions need to be evaluated as the workflow is developed. Does one choose a Gaussian distribution to sample the parameter values? How many sample points are required to fully represent the uncertainties and produce useful probabilistic modeling results without increasing the number of required simulations for real-time applications?

We plan to build upon the approach shown here by adding in the NWP ensembles, following on from the work in *Stefanescu et al.* [2014], to the real-time programming environment highlighted in Figure 6.3. Additionally, we will develop the real-time routines to integrate with different VATD models in a plug-and-play approach as well as with a time-varying version of the 1-D BENT model.

6.5. CONCLUSIONS

Eruptions like Eyjafjallajökull in 2010 [*Gudmundsson et al.*, 2010] can change the landscape for both the scientific and operational hazard-assessment communities. At the time of the 2010 events, there were a request and a need for a better understanding of the uncertainties in the ash-modeling simulations. Meetings such as those reported on in *WMO* [2010a, 2010b, 2013] brought

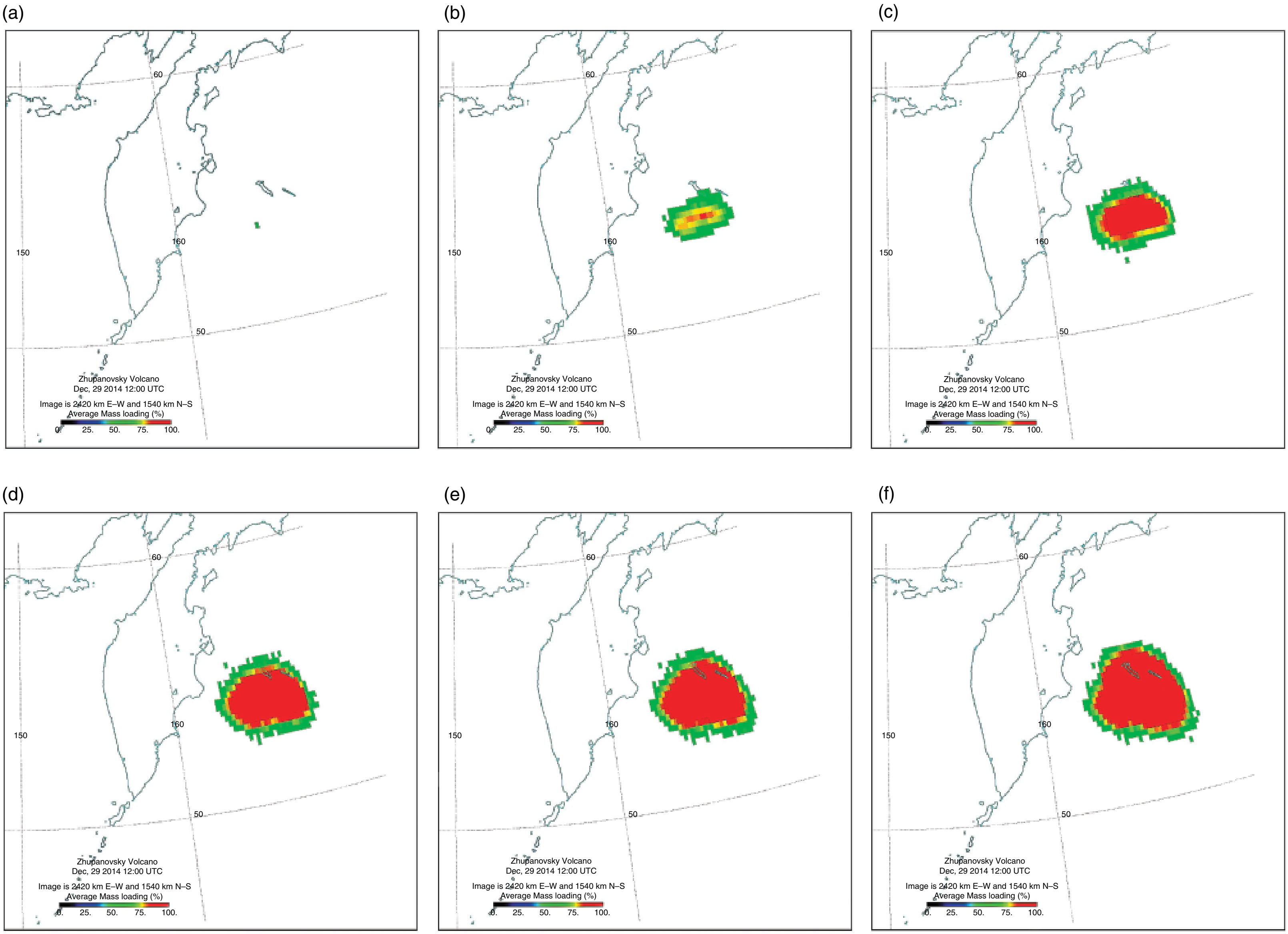

Figure 6.12 Probabilities (%) of volcanic ash mass loading (mg/m^2) exceeding a range of specific thresholds in the simulations for Zhupanovsky volcano, 12:00 UTC 29 December 2014. (a) 100 mg/m^3, (b) 10 mg/m^3, (c) 1 mg/m^3, (d) 0.1 mg/m^3, (e) 0.01 mg/m^3, and (f) 0.001 mg/m^3 or 1 μ mg/m^3.

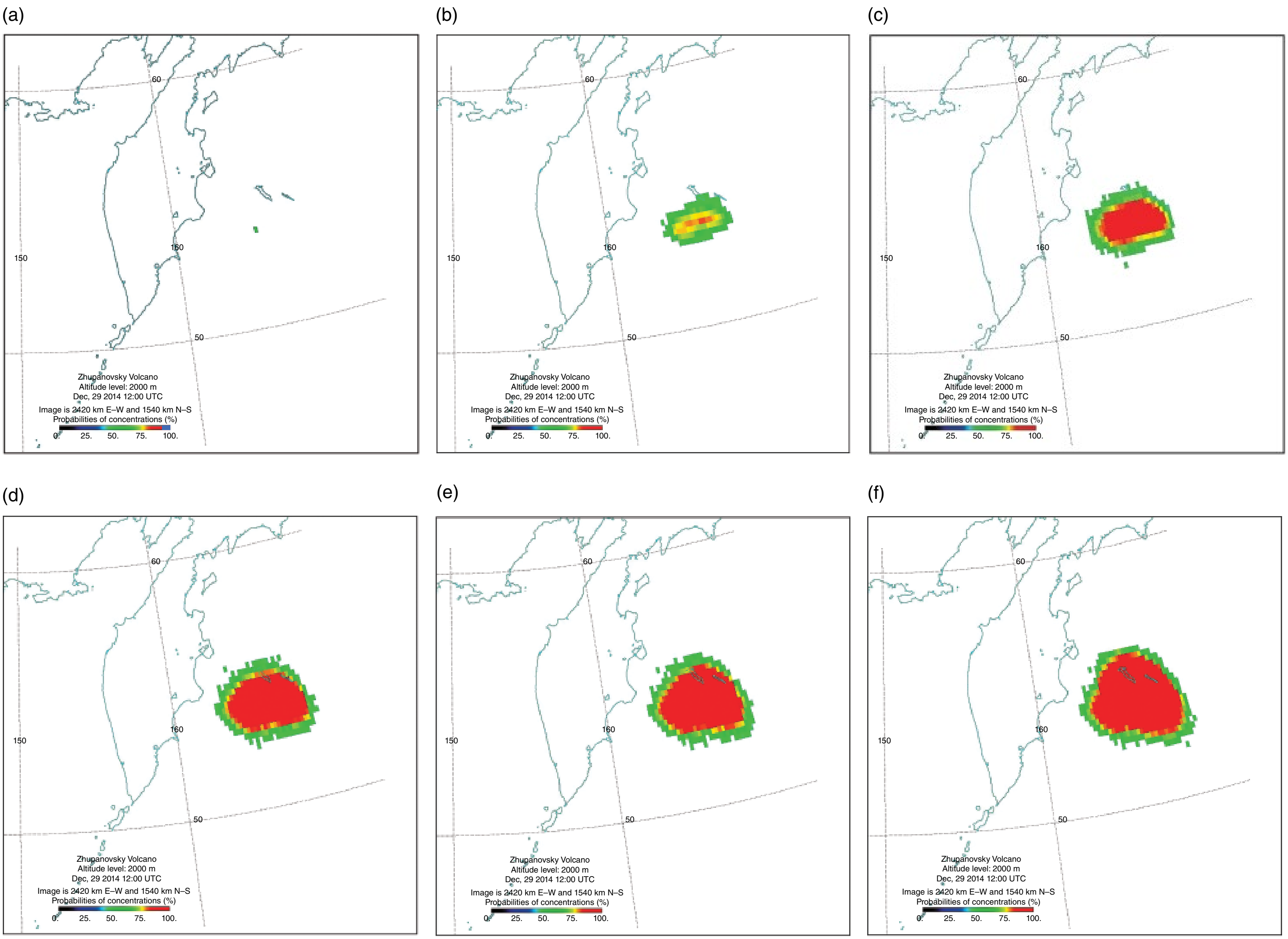

Figure 6.13 Probabilities (%) of volcanic ash concentration (mg/m^3) occurrence at 2 km ASL exceeding a range of specific thresholds in the simulations for Zhupanovsky volcano, 12:00 UTC 29 December 2014, when concentration threshold set at (a) 100 mg/m^3, (b) 10 mg/m^3, (c) 1 mg/m^3, (d) 0.1 mg/m^3, (e) 0.01 mg/m^3, and (f) 0.001 mg/m^3 or 1 μ mg/m^3.

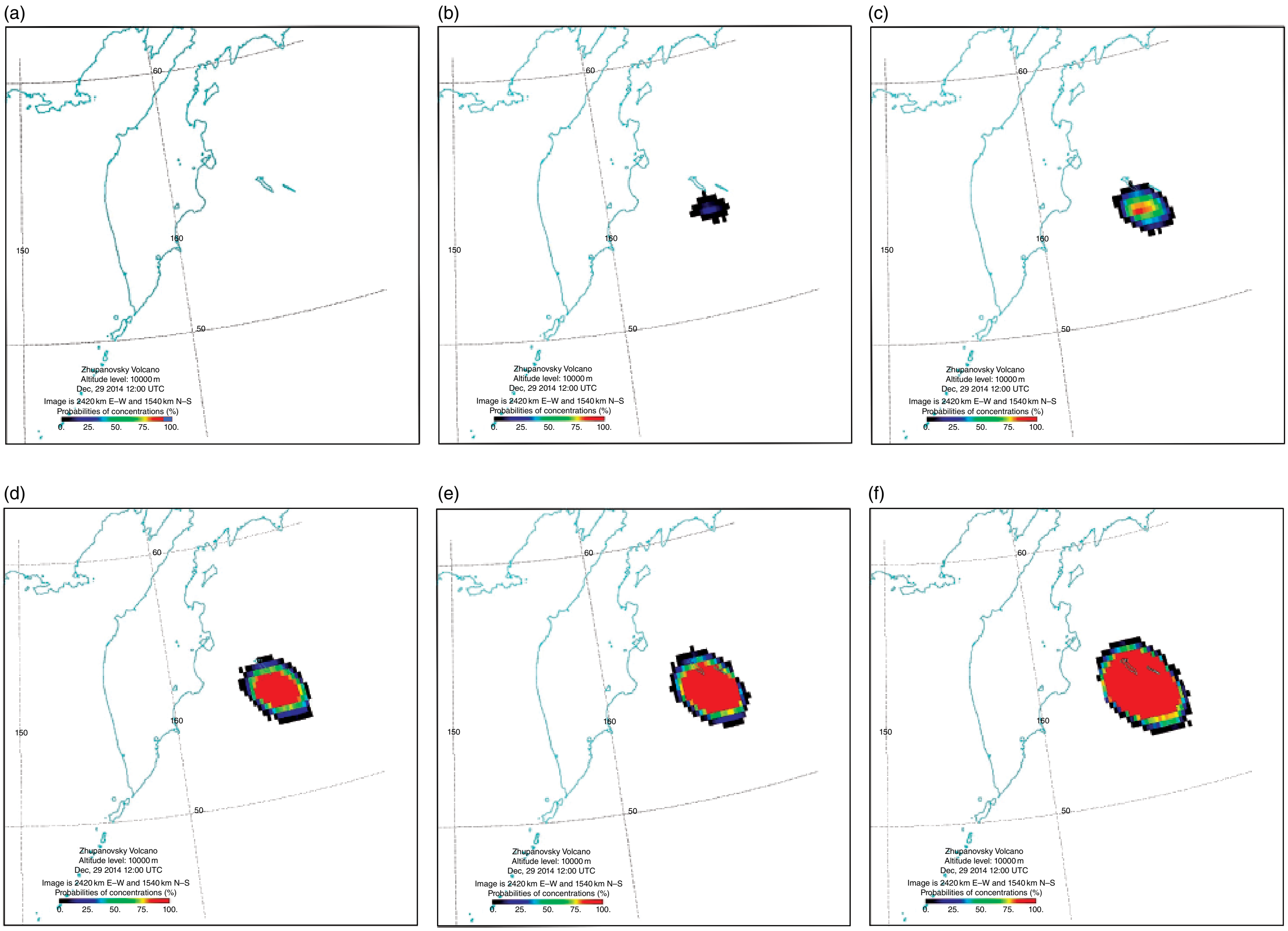

Figure 6.14 Probabilities (%) of volcanic ash concentration (mg/m^3) occurrence at 10 km ASL exceeding a range of specific thresholds in the simulations for Zhupanovsky volcano, 12:00 UTC 29 December 2014, when concentration threshold set at (a) 100 mg/m^3, (b) 10 mg/m^3, (c) 1 mg/m^3, (d) 0.1 mg/m^3, (e) 0.01 mg/m^3, and (f) 0.001 mg/m^3 or 1 μ mg/m^3.

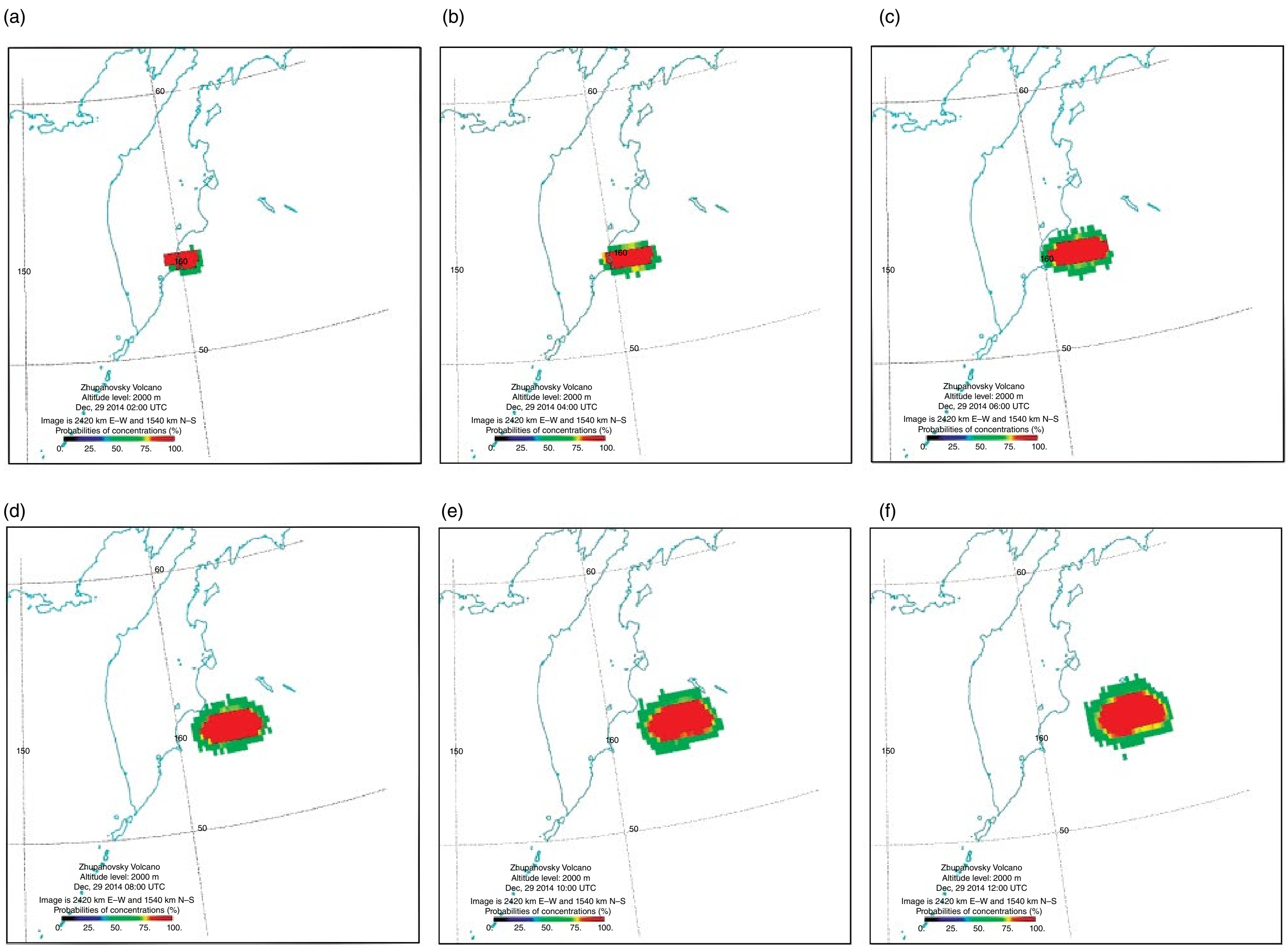

Figure 6.15 Probabilities (%) at 2 km ASL from the simulations for Zhupanovsky volcano, 29 December 2014, when concentrations exceeding at 1 mg/m^3, (a) 02:00, (b) 04:00, (c) 06:00, (d) 08:00, (e) 10:00, and (f) 12:00.

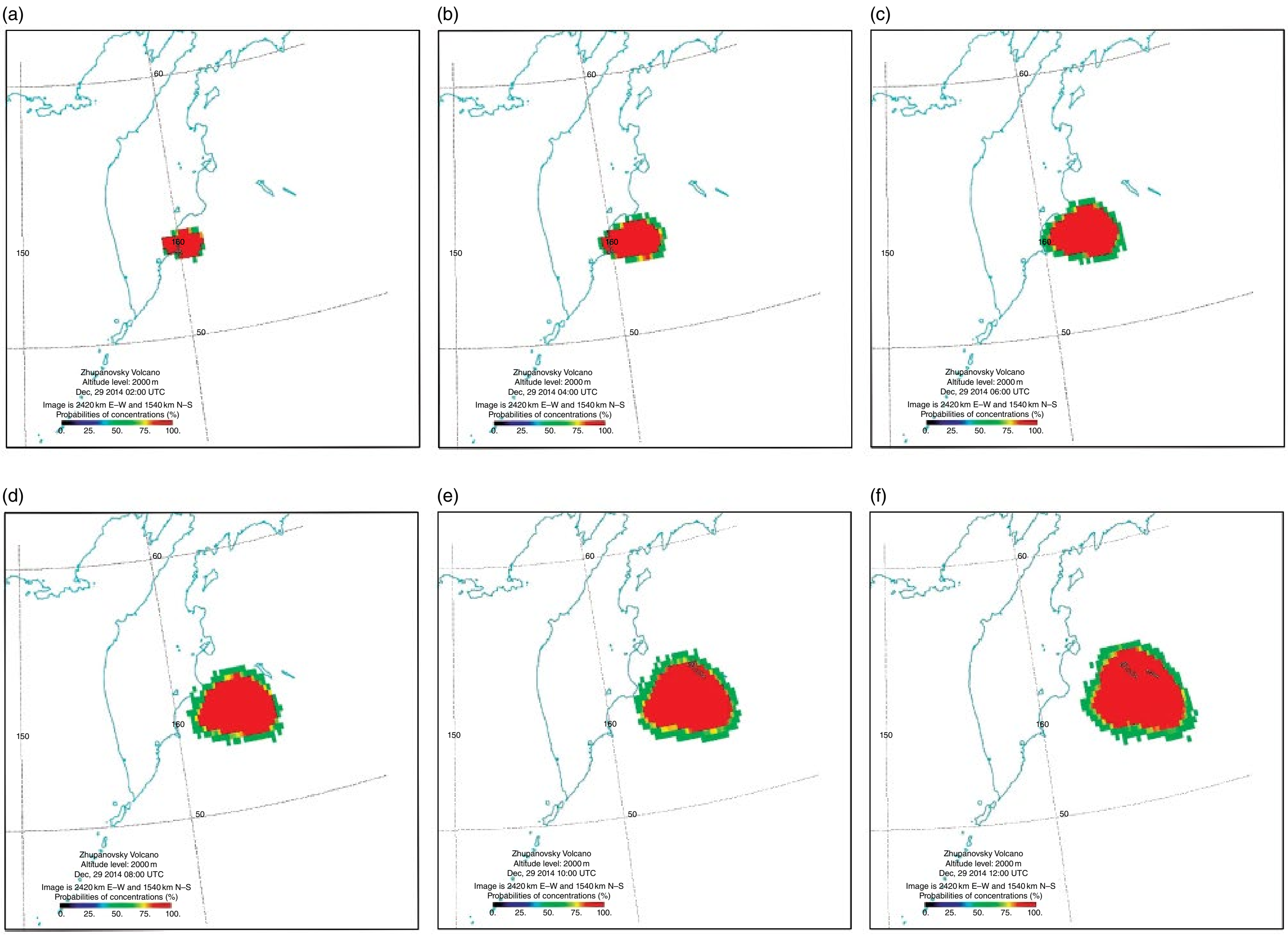

Figure 6.16 Probabilities (%) at 2 km ASL from the simulations for Zhupanovsky volcano, 29 December 2014, when concentrations exceeding at 0.001 mg/m^3, (a) 02:00, (b) 04:00, (c) 06:00, (d) 08:00, (e) 10:00, and (f) 12:00.

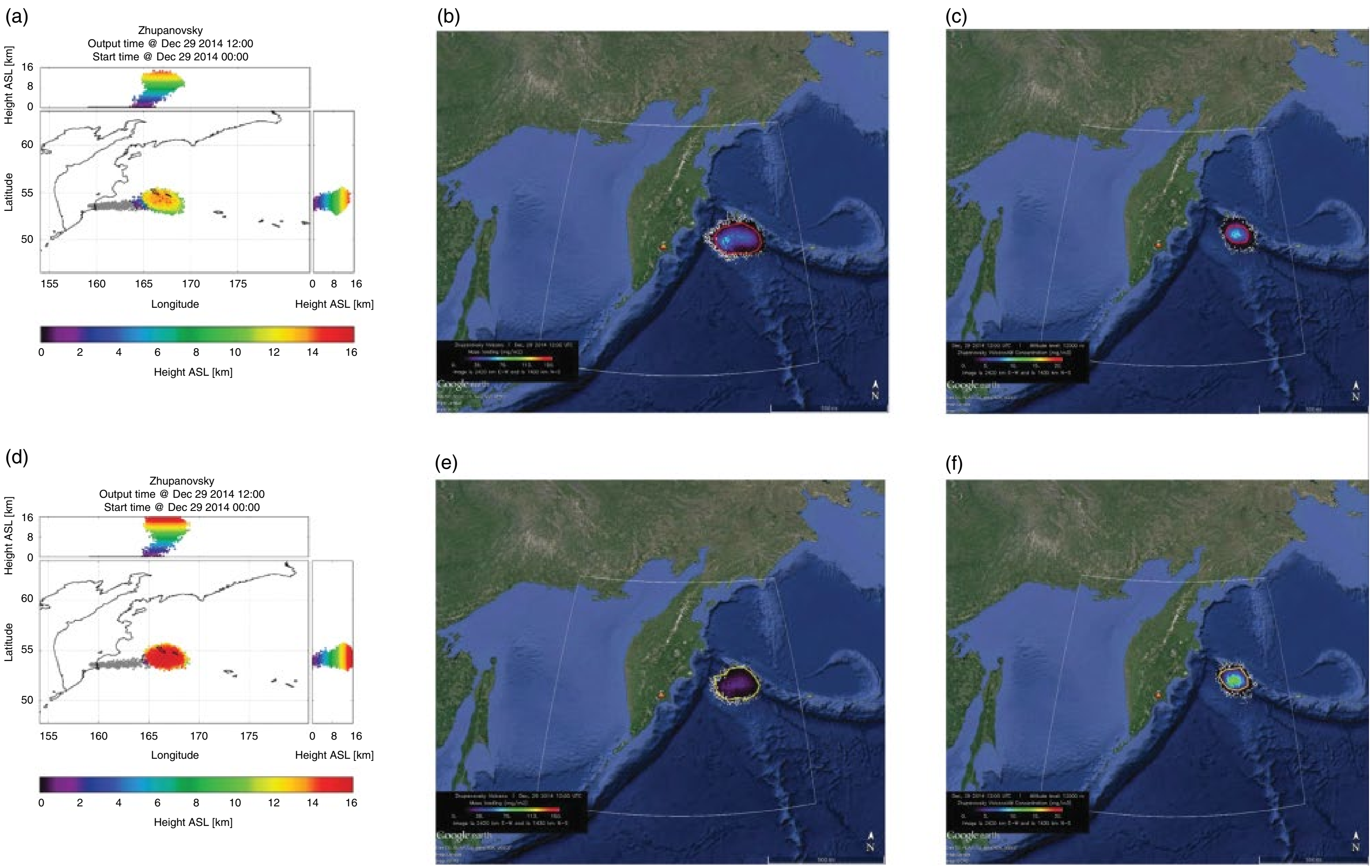

Figure 6.17 Puff volcanic ash cloud simulations #51 and #160, for Zhupanovsky volcano on 29 December 2014 at 12:00 UTC showing Puff particle locations ([a] for #51; [d] for #160), mass loadings ([b] for #51; [e] for #160), and ash concentrations from 10 to 12 km ASL ([c] for #51; [f] for #160).

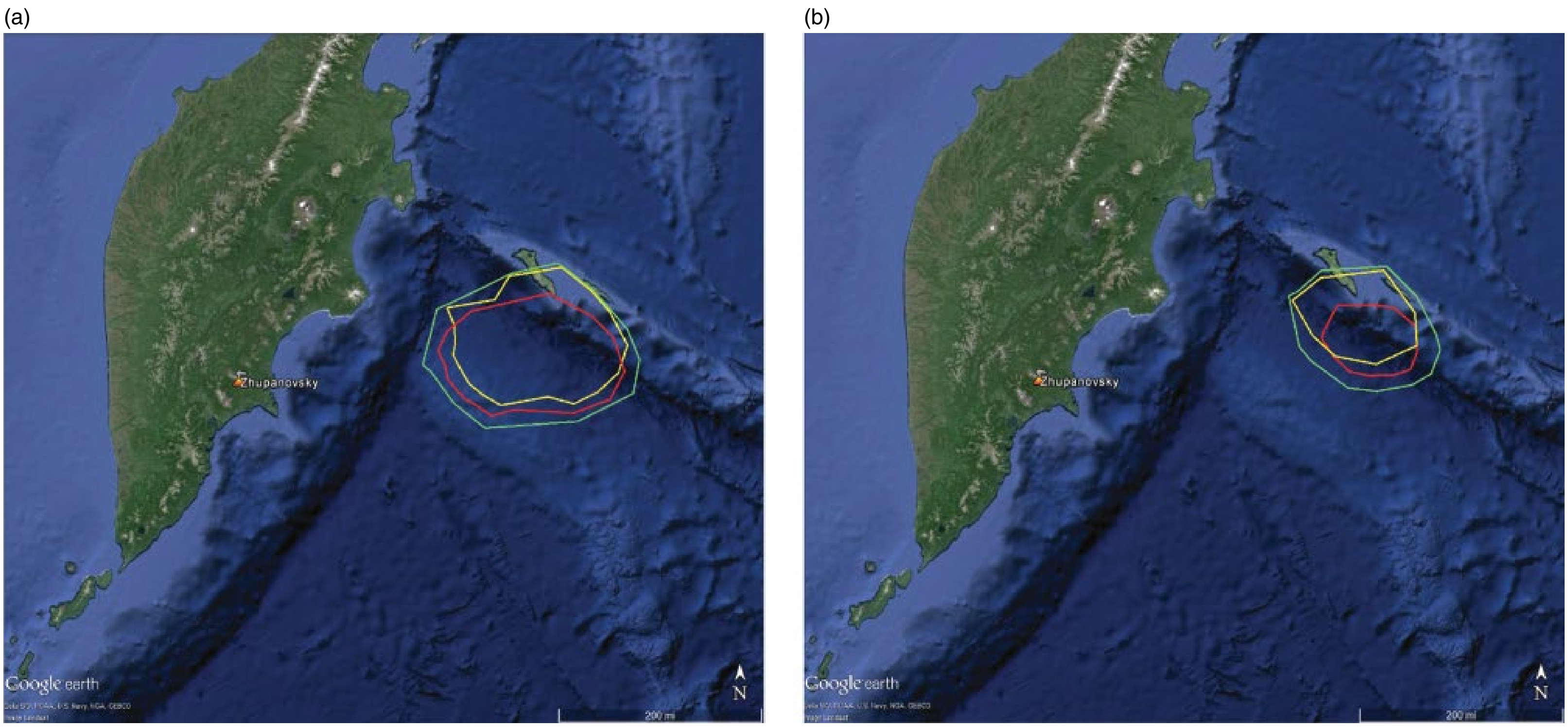

Figure 6.18 Polygons for simulation #51 and #160 for Zhupanovsky volcano on 29 December 2014 at 12:00 UTC. (a) Mass loadings for #51, yellow polygon, and #161, red polygon, as well as the mean from all simulation members, green polygon. (b) Ash concentrations at 10–12 km ASL for #51, yellow polygon, and #161, red polygon as well as the mean from all simulation members, green polygon.

together these two communities where a common theme emerged on the need to move from deterministic modeling to combined deterministic and probabilistic approach. As *WMO* [2013] states, certain eruption source parameters, such as plume height (km ASL) and eruption length (s), can be measured during the event while others, such as eruption rate (m^3/s) and particle size distribution, can either be estimated from past eruptions or derived directly from the measured eruption data.

We presented a workflow for probabilistic modeling where a 1-D plume rise model, BENT [*Bursik,* 2001] has been coupled to a four-dimensional volcanic-ash transport and dispersion (VATD) model. We focused on four BENT model parameters to build our probabilistic modeling approach. We built a complete workflow that coupled the input uncertainties from the 161 simulation members with the Puffin tool to develop downwind atmospheric ash concentrations and mass loadings with the associated probabilities of exceeding specific thresholds. We have shown how, in using our system, maps of the mean ash-mass loadings with time from our 161 simulation members can be produced along with probabilities of exceeding defined ash-mass loadings and atmospheric ash-concentration thresholds. Being able to quantify the likelihood of exceeding a specific concentration or mass loading threshold delivers a new tool for those in real-time ash-cloud hazard assessment to add to their advisories needed for aviation safety and human health impact.

However, the more critical question is how to communicate these probabilities to the end user and how to transition the research to operations? What does it mean to say that half of the 161 members breached the threshold? How would a 95% probability of exceeding a mass loading of 1 mg/m^2 in a model simulation be used in a VAA by a VAAC forecaster? How would this information be interpreted by the aviation community? Our modeling results could be compared and evaluated with available remote sensing data to provide additional tools as the VAAC produces its VAA and VAG. To fully develop these probabilistic tools so they can move directly from research to operations requires the research community to demonstrate how the probabilistic modeling provides additional and useful information on the dispersing cloud that can then assist in the advisories produced by each VAAC.

Learning from the NWP community in how they use and communicate probabilities from their ensemble member NWP model simulations, such as *Roebber et al.* [2004], will be critical in how the probabilistic modeling approach is used in real-time volcanic ash-cloud hazard assessment. To develop a probabilistic approach into a real-time system that can produce results in a timely manner is as important as the research itself into the probabilistic analysis techniques and sensitivity of dispersion results. If the computation takes too long or has not been developed to integrate with operational hazard assessment tools in the VAAC, then it will be very difficult for the operators to use the tool. Working directly with those in operations and supporting them on the integration of the tool as the probabilistic modeling system is developed means that the final product can be used from day one of operations.

ACKNOWLEDGMENTS

This work was funded by National Science Foundation (NSF) Interdisciplinary/Collaborative Research under grant no. CMMI-1131799. We would like to thank Dr. Donald Morton, Arctic Region Supercomputing Centre, Geophysical Institute, UAF, for his assistance on the NSF IDR project and Dr. Rorik Peterson, College of Engineering and Mines, UAF, for his time and expertise in building the MPI version of the Puff VATD model. We thank the Vhub team for housing the Puffin interface for users of the tool and for providing the computing support for the NSF IDR project discussions and meeting notes. Finally, we would like to thank the editors in chief and associate editors of the American Geophysical Union monograph series for the opportunity to publish this manuscript and for bringing all the different manuscripts together to develop such a unique and diverse publication.

REFERENCES

Alaska Volcano Observatory (AVO) (2014), Cleveland Volcano: Current Volcanic Activity, http://avo.alaska.edu/activity/Cleveland.php, last viewed 9 January 2015.

Bursik, M. (2001), Effect of wind on the rise height of volcanic plumes, *Geophys. Res. Lett.*, *28*(18), 3621–3624.

Bursik, M., M. Jones, S. Carn, K. Dean, A. Patra, M. Pavolonis, E. B. Pitman, T. Singh, P. Singla, P. Webley, H. Bjornsson, and M. Ripepe (2012), Estimation and propagation of volcanic source parameter uncertainty in an ash transport and dispersal model: application to the Eyjafjallajökull plume of 14–16 April 2010, *Bull. Volcanol.*, *74*(10), 2321–2338.

Ellrod, G. P., B. H. Connell, and D. W. Hillger (2003), Improved detection of airborne volcanic ash using multispectral infrared satellite data, *J. Geophys. Res. Atmos. (1984–2012)*, *108* (D12); doi: 10.1029/2002JD002802.

Folch, A., A. Costa, and S. Basart, (2012), Validation of the FALL3D ash dispersion model using observations of the 2010 Eyjafjallajökull volcanic ash clouds, *Atmos. Environ.*, *48*, 165–183.

Gudmundsson, M. T., R. Pedersen, K. Vogfjörd, B. Thorbjarnardóttir, S. Jakobsdóttir, and M. J. Roberts, (2010), Eruptions of Eyjafjallajökull Volcano, Iceland, *Eos, Trans. AGU*, *91*(21), 190–191.

Gudmundsson, M. T., T. Thordarson, Á. Höskuldsson, G. Larsen, H. Björnsson, F. J. Prata, B. Oddsson, E. Magnússon, T. Högnadóttir, G. N. Petersen, C. L. Hayward, J. A. Stevenson, and I. Jónsdóttir (2012), Ash generation and distribution from the April–May 2010 eruption of Eyjafjallajökull, Iceland, *Sci. Rep.*, *2*.

Guffanti, M., and A. Tupper (2014), Chapter 4, Volcanic ash hazards and aviation risk, *Volcanic Hazards, Risks and Disasters,* edited by P. Papale and J. F. Shroder, 87–105.

Global Volcanism Program (GVP) (2015), Weekly activity report, 31 December 2014–6 January 2015; http://www.volcano.si.edu/reports_weekly.cfm#vn_211060, last viewed 9 January 2015.

Horwell, C. J., and P. J. Baxter (2006), The respiratory health hazards of volcanic ash: a review for volcanic risk mitigation, *Bull. Volcanol.*, *69*(1), 1–24.

International Civil Aviation Agency (ICAO) (2012), International Volcanic Ash Task Force, http://www.icao.int/safety/meteorology/ivatf/Pages/default.aspx, last viewed 8 January 2015.

Japanese Meteorology Agency (JMA) (2014), Tokyo Volcanic Ash Advisory Center, http://ds.data.jma.go.jp/svd/vaac/data/index.html, last viewed 8 January 2015.

Madankan, R., S. Pouget, P. Singla, M. Bursik, J. Dehn, M. Jones, A. Patra, M. Pavolonis, E. B. Pitman, T. Singh, and P. Webley (2014), Computation of probabilistic hazard maps and source parameter estimation for volcanic ash transport and dispersion, *J. Computational Phys.*, *271*, 39–59.

Meteorological Office (2012), The volcanic ash modelling setup: London VAAC, viewed 8 January 2015; http://www.metoffice.gov.uk/media/pdf/p/7/London_VAAC_Current_Modelling_SetUp_v01-1_05042012.pdf.

Patra, A. K., M. Bursik, J. Dehn, M. Jones, R. Madankan, D. Morton, M. Pavolonis, E. B. Pitman, S. Pouget, T. Singh, P. Singla, E. R. Stefanescu, and P. Webley (2013), Challenges in developing DDDAS based methodology for volcanic ash hazard analysis–effect of numerical weather prediction variability and parameter estimation, *Procedia Computer Sci.*, *18*, 1871–1880.

Pavolonis, M. J., A. K. Heidinger, and J. Sieglaff (2013), Automated retrievals of volcanic ash and dust cloud properties from upwelling infrared measurements, *J. Geophys. Res. Atmos.*, *118*(3), 1436–1458.

Prata, A. J., and A. Tupper (2009), Aviation hazards from volcanoes: The state of the science, *Nat. Hazards*, *51*(2), 239–244.

Roebber, P. J., D. M. Schultz, B. A. Colle, and D. J. Stensrud (2004), Toward improved prediction: High-resolution and ensemble modeling systems in operations, *Weath. Forecast.*, *19*(5), 936–949.

Schneider, D. J., and R. P. Hoblitt (2013), Doppler weather radar observations of the 2009 eruption of Redoubt Volcano, Alaska, *J. Volcanol. Geotherm. Res.*, *259*, 133–144.

Searcy, C., K. Dean, and W. Stringer (1998), PUFF: A high-resolution volcanic ash tracking model, *J. Volcanol. Geotherm. Res.*, *80*(1), 1–16.

Steensen, T., M. Stuefer, P. Webley, G. Grell, and S. Freitas (2013), Qualitative comparison of Mount Redoubt 2009 volcanic clouds using the PUFF and WRF-Chem dispersion models and satellite remote sensing data, *J. Volcanol. Geotherm. Res.*, *259*, 235–247.

Stefanescu, E. R., A. K. Patra, M. I. Bursik, R. Madankan, S. Pouget, M. Jones, P. Singla, T. Singh, E. B. Pitman, M. Pavolonis, D. Morton, P. Webley, and J. Dehn (2014), Temporal, probabilistic mapping of ash clouds using windfield stochastic variability and uncertain eruption source parameters: Example of the 14 April 2010 Eyjafjallajökull eruption, *J. Adv. Model. Earth Syst.*, *6*(4), 1173–1184.

Tesche, M., P. Glantz, C. Johansson, M. Norman, A. Hiebsch, A. Ansmann, D. Althausen, R. Engelmann, and P. Seifert (2012), Volcanic ash over Scandinavia originating from the Grímsvötn eruptions in May 2011, *J. Geophys. Res. Atmos. (1984–2012)*, *117*(D9).

Vogel, H., J. Förstner, B. Vogel, T. Hanisch, B. Mühr, U. Schättler, and T. Schad (2014), Time-lagged ensemble simulations of the dispersion of the Eyjafjallajökull plume over Europe with COSMO-ART, *Atmos. Chem. Phys.*, *14*, 7837–7845; doi:10.5194/acp-14-7837-2014.

Weber, K., J. Eliasson, A. Vogel, C. Fischer, T. Pohl, G. van Haren, M. Meier, B. Grobety, and D. Dahmann (2012), Airborne in-situ investigations of the Eyjafjallajökull volcanic ash plume on Iceland and over north-western Germany with light aircrafts and optical particle counters, *Atmos. Environ.*, *48*, 9–21.

Webley, P. W., B. J. B. Stunder, and K. G. Dean (2009a), Preliminary sensitivity study of eruption source parameters for operational volcanic ash cloud transport and dispersion models: A case study of the August 1992 eruption of the Crater Peak vent, Mount Spurr, Alaska, *J. Volcanol. Geotherm. Res.*, *186*(1), 108–119.

Webley, P. W., K. Dean, J. E. Bailey, J. Dehn, and R. Peterson (2009b), Automated forecasting of volcanic ash dispersion utilizing Virtual Globes, *Nat. Hazards*, *51*(2), 345–361.

Webley, P. W., K. Dean, R. Peterson, A. Steffke, M. Harrild, and J. Groves (2012), Dispersion modeling of volcanic ash clouds: North Pacific eruptions, the past 40 years: 1970–2010, *Nat. Hazards*, *61*(2), 661–671.

Webley, P. W., K. G., Dean, J. Dehn, J. E. Bailey, and R. Peterson (2010), Volcanic-ash dispersion modeling of the 2006 eruption of Augustine volcano using the Puff model, chapter 21 of J. A. Power, M. L. Coombs, and J. T. Freymueller, eds., The 2006 eruption of Augustine Volcano, Alaska, U.S. Geological Survey Professional Paper 1769, 482–501.

Witham, C. S., M. C. Hort, R. Potts, R. Servranckx, P. Husson, and F. Bonnardot (2007), Comparison of VAAC atmospheric dispersion models using the 1 November 2004 Grímsvötn eruption, *Meteor. App.*, *14*(1), 27–38.

World Meteorological Organization (WMO) (2010a), Workshop on ash dispersal forecast and civil aviation:

Results from the 1st Workshop, Model Definition Document, last viewed 8 January 2015; http://www.unige.ch/sciences/terre/mineral/CERG/Workshop/results/Model-Document-Geneva10.pdf.

World Meteorological Organization (WMO) (2010b), Workshop on Ash Dispersal Forecast and Civil Aviation: Results from the 1st Workshop: Benchmark Document, last viewed 8 January 2015; http://www.unige.ch/sciences/terre/mineral/CERG/Workshop/results/ADCAW2010-benchmark-doc.pdf.

World Meteorological Organization (WMO) (2013), Workshop on Ash Dispersal Forecast and Civil Aviation: Results from the 2nd Workshop: Updated model definition document, viewed 8 January 2015; http://www.unige.ch/sciences/terre/mineral/CERG/Workshop2/results-2/Model-Definition-Document-2013.pdf.